J|A|C|S
ARTICLES
Published on Web 02/25/2003

Catalytic Gas Phase Oxidation of Methanol to Formaldehyde

Tom Waters, Richard A. J. O'Hair,* and Anthony G. Wedd

Contribution from the School of Chemistry, The University of Melbourne, Parkville, Victoria, Australia, 3010

Received October 7, 2002; E-mail: rohair@unimelb.edu.au

Abstract: Two gas-phase catalytic cycles for the two-electron oxidation of primary and secondary alcohols were detected by multistage mass spectrometry experiments. A binuclear dimolybdate center $[Mo_2O_6(OCHR_2)]^-$ acts as the catalyst in both these cycles. The first cycle proceeds via three steps: (1) reaction of $[Mo_2O_6(OH)]^-$ with alcohol R_2HCOH and elimination of water to form $[Mo_2O_6(OCHR_2)]^-$; (2) oxidation of the alkoxo ligand and its elimination as aldehyde or ketone in the rate-determining step; and (3) regeneration of the catalyst via oxidation by nitromethane. Step 2 does not occur at room temperature and requires the use of collisional activation to proceed. The second cycle is similar but differs in the order of reaction with alcohol and nitromethane. The nature of each of these reactions was probed by kinetic measurements and by variation of the substrate alcohols (structure and isotope labeling). The role of the binuclear molybdenum center was assessed by examination of the relative reactivities of the mononuclear $[MO_3(OH)]^-$ and binuclear $[M_2O_6(OH)]^-$ ions (M = Cr, Mo, W). The molybdenum and tungsten binuclear centers $[M_2O_6(OH)]^-$ (M = Mo, W) were reactive toward alcohol but the chromium center $[Cr_2O_6(OH)]^-$ was not. This is consistent with the expected order of basicity of the hydroxo ligand in these species. The chromium and molybdenum centers $[M_2O_6(OCHR_2)]^-$ (M = Cr, Mo) oxidized the alkoxo ligand to aldehyde, while the tungsten center $[W_2O_6(OCHR_2)]^-$ did not, instead preferring the non-redox elimination of alkene. This is consistent with the expected order of oxidizing power of the anions. Each of the mononuclear anions $[MO_3(OH)]^-$ (M = Cr, Mo, W) was inert to reaction with methanol, highlighting the importance of the second MoO_3 unit in these catalytic cycles. Only the dimolybdate center has the mix of properties that allow it to participate in *each* of the three steps of the two catalytic cycles. The three reactions of these cycles are equivalent to the three essential steps proposed to occur in the industrial oxidation of gaseous methanol to formaldehyde at 300−400 °C over solid-state catalysts based upon molybdenum(VI)-trioxide. The new gas-phase catalytic data is compared with those for the heterogeneous process.

Introduction

Synthetic catalysts contribute to an estimated one-sixth of the value of all manufactured goods in industrialized countries.[1] Inorganic catalysts are crucial to production of organic chemicals and petroleum products, and are playing an increasing role in development of alternative and cleaner industrial processes. However, the detailed molecular mechanisms of many important catalytic processes remain obscure. It has become apparent that gas-phase studies employing multistage mass spectrometry can be exploited to provide insights into the elementary steps of catalysis.[2]

Coordinatively unsaturated gas-phase transition metal-oxo fragment ions often display little selectivity for bond activation.[3] For example, the reaction of MoO_2^+ with methanol gives rise to four different reaction channels involving activation of C−H, C−O, and O−H bonds.[4,5] However, electrospray ionization (ESI) permits transfer of metal-oxo ions from condensed phases to the gas phase, allowing comparison of reactivity of ions that exist in both the gaseous and condensed phases.[6] We now report a detailed study of the catalytic oxidation of methanol to formaldehyde in the gas phase by an anionic dimolybdate(VI) center using multistage mass spectrometry experiments (Figure 1, reactions 1−5).[7] In a preliminary communication, similarities were noted between this gas-phase catalysis (eq 6) and that

(1) Shriver, D. F.; Atkins, P. W.; Langford, C. H. *Inorganic Chemistry*, 2nd ed.; Oxford University Press: Oxford, 1994; Chapter 17, p 709.
(2) (a) Plattner, D. A. *Int. J. Mass Spectrom.* **2001**, *207*, 125. **(b)** Zemski, K. A.; Justes, D. R.; Castleman, A. W., Jr. *J. Phys. Chem. B* **2002**, *106*, 6136.
(3) (a) Schröder, D.; Schwarz, H. *Angew. Chem., Int. Ed. Engl.* **1995**, *34*, 1973. (b) Schröder, D.; Schwarz, H.; Shaik, S. In *Metal-Oxo and Metal-Peroxo Species in Catalytic Oxidations*; Meunier, B., Ed.; Springer: Berlin, 2000; *Struct. Bond.*; Vol. 97, p 91.
(4) (a) Fialko, E. F.; Kikhtenko, A. V.; Goncharov, V. B.; Zamaraev, K. I. *J. Phys. Chem. B* **1997**, *101*, 5772. (b) Fialko, E. F.; Kikhtenko, A. V.; Goncharov, V. B. *Organometallics*, **1998**, *17*, 25.
(5) For a selection of other studies on the gas-phase chemistry of molybdenum oxo species, see: (a) Cassady, C. J.; McElvany, S. W. *Organometallics*, **1992**, *11*, 2367. (b) Keesee, R. G.; Chen, B.; Harms, A. C.; Castleman, A. W., Jr. *Int. J. Mass Spectrom. Ion Proc.* **1993**, *123*, 225. (c) Kretzschmar, I.; Fiedler, A.; Harvey, J. N.; Schröder, D.; Schwarz, H. *J. Phys. Chem. A* **1997**, *101*, 6252. (d) Fialko, E. F.; Kikhtenko, A. V.; Goncharov, V. B.; Zamaraev, K. I.; *J. Phys. Chem. A* **1997**, *101*, 8607. (e) Sievers, M. R.; Armentrout, P. B. *J. Phys. Chem. A* **1998**, *102*, 10 754.
(6) For a selection of studies that have used ESI to transfer metal-oxide anions to the gas phase, see (a) Lau, T.-C.; Wang, J.; Siu, K. W. M.; Guevremont, R. *Chem. Commun.* **1994**, 1487. (b) Deery, M. J.; Howarth, O. W.; Jennings, K. R. *J. Chem. Soc., Dalton Trans.* **1997**, 4783. (c) Walanda, D. K.; Burns, R. C.; Lawrance, G. A.; von Nagy-Felsobuki, E. I. *J. Chem. Soc., Dalton Trans.* **1999**, 311. (d) Truebenbach, C. S.; Houalla, M.; Hercules, D. M. *J. Mass Spectrom.* **2000**, *35*, 1121.

10.1021/ja028839x CCC: $25.00

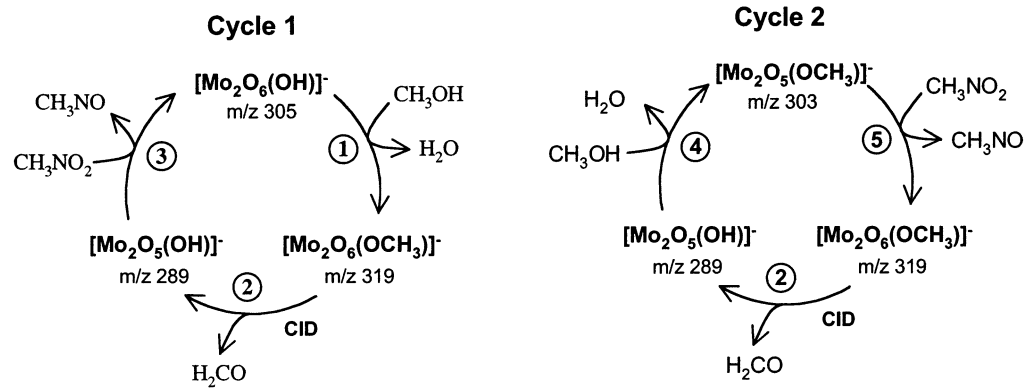

Figure 1. Gas-phase catalytic cycles for the oxidation of methanol to formaldehyde. Reactions are numbered and described in the text. Reaction 2 links $[Mo_2O_6(OCH_3)]^-$ (*m*/*z* 319) and $[Mo_2O_5(OH)]^-$ (*m*/*z* 289) and appears in both cycles. Cycles 1 and 2 differ in the sequence of reaction with CH_3NO_2 and CH_3OH. Quoted *m*/*z* values refer to a single peak selected from the dimolybdate isotope manifold and followed through relevant reactions.

occurring in the industrial oxidation of methanol to formaldehyde over solid-state molybdenum(VI) oxide catalysts (eq 7)[8]

$$CH_3OH + CH_3NO_2 \rightarrow H_2CO + H_2O + CH_3NO \quad (6)$$

$$CH_3OH + 1/2\ O_2 \rightarrow H_2CO + H_2O \quad (7)$$

Due to the industrial and economic importance of formaldehyde,[9] the partial oxidation of methanol over molybdenum(VI) oxide based catalysts[10] has been the subject of detailed studies employing a wide variety of synthetic, kinetic, spectroscopic and theoretical techniques.[11−14] The process can be divided into three essential steps:[15]

(i) Gaseous methanol undergoes dissociative adsorption on the surface of the solid-state catalyst to yield surface methoxomolybdenum(VI) centers. Water may be desorbed from the catalyst in this step.

(ii) The activated methoxo ligands are oxidized and eliminated as formaldehyde, resulting in the reduction of the catalyst and the creation of an oxygen vacancy. This step is rate determining and elevated temperatures are required.

(iii) Oxidation of the bulk catalyst by dioxygen completes the cycle.

Although there is qualitative agreement regarding key reactions and intermediates in this process, a detailed *molecular* understanding of the elementary reactions has been elusive. Reactions equivalent to steps i−iii above are described in the gas-phase cycles of Figure 1 (reactions 1−5). Two cycles are presented, differing in the sequence of reactions. The role of the binuclear molybdenum center was assessed by examination of the relative reactivities of the mononuclear $[MO_3(OH)]^-$ and binuclear $[M_2O_6(OH)]^-$, (M = Cr, Mo, W) ions.

Experimental Section

Synthesis. Tetra-*n*-butylammonium (Bu_4N^+) salts of $[Cr_2O_7]^{2-}$, $[Mo_2O_7]^{2-}$, $[CrO_4]^{2-}$, $[MoO_4]^{2-}$, and $[WO_4]^{2-}$ were synthesized using standard literature methods.[16−20]

Reagents. Methanol, ethanol, *n*-propanol, *i*-propanol, and *tert*-butyl alcohol (HPLC grade, 99.5%) were obtained from Aldrich and used without further purification. CF_3CH_2OH (99.5%) was obtained from ICN Biomedicals. CFH_2CH_2OH (95%) was obtained from Lancaster. CH_3OD (99.5 atom % D), CD_3OD (99.8 atom % D), CD_3CH_2OH (99 atom % D) and CH_3CD_2OH (98 atom % D) were obtained from Aldrich. $CH_3{}^{18}OH$ (95 atom % ^{18}O) was obtained from Isotec. CH_3CHDOH was synthesized using a standard literature procedure[21] and characterized by NMR. Acetonitrile (HPLC grade, 99.8%) was obtained from Merck.

Mass Spectrometry. Mass spectrometry experiments were conducted using a modified Finigan LCQ quadrupole ion trap mass spectrometer equipped with a Finnigan electrospray ionization source. Tetrabutylammonium salts of metal-oxide anions were dissolved in acetonitrile (0.1 mg/mL). The solution was pumped into the electrospray source at approximately 3 μL/min. Typical electrospray source conditions involved needle potentials of 3.5−4.0 kV and heated capillary temperatures of 150−250 °C. Extensive tuning of electrospray conditions was often required due to the low signal-to-noise ratio and/or low abundance of some species. Mass selection and collisional

(7) A number of gas-phase catalytic cycles have been established using mass spectrometry. See for example: oxidation of CO (a) Kappes, M. M.; Staley, R. H. *J. Am. Chem. Soc.* **1981**, *103*, 1286. (b) Baranov, V.; Javahery, G.; Hopkinson, A. C.; Bohme, D. K. *J. Am. Chem. Soc.* **1995**, *117*, 12 801. (c) Shi, Y.; Ervin, K. M. *J. Chem. Phys.* **1998**, *108*, 1757; oxidation of methane. (d) Wesendrup, R.; Schröder, D.; Schwarz, H. *Angew. Chem., Int. Ed. Engl.* **1994**, *33*, 1174; and formation of benzene from ethene. (e) Schnabel, P.; Irion, M. P.; Weil, K. G. *J. Phys. Chem.* **1991**, *95*, 9688.
(8) Waters, T.; O'Hair, R. A. J.; Wedd, A. G. *Chem. Commun*. **2000**, 225.
(9) The huge demand for formaldehyde-based resins for particleboard wood products makes formaldehyde one of the top 25 chemicals produced in industrial countries, with approximately 15 million metric tons of formaldehyde (37% aqueous solution) produced annually. See for example: Gerberich, H. R.; Seaman, G. C. *Formaldehyde* in *Kirk-Othmer Encyclopedia of Chemical Technology*, 4th ed.; Howe-Grant, M., Ed.; John Wiley and Sons: New York, 1994; vol. 11, p 929−950.
(10) A molybdenum(VI) trioxide-based catalyst or a metallic silver catalyst is used. About 70% of newly installed production capacity uses the former. The heterogeneous catalysis is typically carried out at atmospheric pressure and 300−400 °C with atmospheric dioxygen as the oxidant. High methanol conversion (>99%) and selectivity for formaldehyde (>95%) can be achieved. *ibid.*
(11) (a) McCarron, E. M., III.; Staley, R. H.; Sleight, A. W. *Inorg. Chem.* **1984**, *23*, 1043. (b) McCarron, E. M., III.; Sleight, A. W. *Polyhedron*, **1986**, *5*, 129. (c) McCarron, E. M., III.; Harlow, R. L.; Li, Z. G.; Suto, C.; Yuen, Y. *J. Solid State Chem.* **1998**, *136*, 247.
(12) (a) Holstein, W. L.; Machiels, C. J. *J. Catal.* **1996**, *162*, 118. (b) Ardissone, D. E.; Valente, N. G.; Cadús, L. E.; Arrúa, L. A. *Ind. Eng. Chem. Res.* **2000**, *39*, 2902. (c) Faliks, A.; Yetter, R. A.; Floudas, C. A.; Bernasek, S. L.; Fransson, M.; Rabitz, H. *J. Phys. Chem. A* **2001**, *105*, 2099.
(13) See for example: (a) Groff, R. P. *J. Catal.* **1984**, *86*, 215. (b) Hu, H.; Wachs, I. E.; Bare, S. R. *J. Phys. Chem.* **1995**, *99*, 10 897. (c) Zhang, W.; Desikan, A.; Oyama, S. T. *J. Phys. Chem.* **1995**, *99*, 14 468. (d) Radhakrishnan, R.; Reed, C.; Oyama, S. T.; Seman, M.; Knodo, J. N.; Domen, K.; Ohminami, Y.; Asakura, K. *J. Phys. Chem. B* **2001**, *105*, 8519. (e) Burcham, L. J.; Briand, L. E.; Wachs, I. E. *Langmuir*, **2001**, *17*, 6164.
(14) (a) Allison, J. N.; Goddard, W. A., III *J. Catal.* **1985**, *92*, 127. (b) Weber, R. S. *J. Phys. Chem.* **1994**, *98*, 2999. (c) Rahmouni, A.; Barbier, C. *J. Mol. Struct. (THEOCHEM)*, **1995**, *330*, 359.
(15) (a) Farneth, W. E.; Ohuchi, F.; Staley, R. H.; Chowdhry, U.; Sleight, A. W. *J. Phys. Chem.* **1985**, *89*, 2493. (b) Farneth, W. E.; Staley, R. H.; Sleight, A. W. *J. Am. Chem. Soc.* **1986**, *108*, 2327.
(16) Landini, D.; Rolla, F. *Chem. Indust.*, **1979**, 213.
(17) Hur, N. H.; Klemperer, W. G.; Wang, R.-C. In *Inorganic Synthesis*; Ginsberg, A. P. Ed.; John Wiley & Sons: New York, 1990; Vol. 27, p 79−80.
(18) Nakayama, H. *Bull. Chem. Soc. Jpn.* **1983**, *56*, 877.
(19) Klemperer, W. G.; Liu, R.-S. *Inorg. Chem.* **1980**, *19*, 3863.
(20) Che, T. M.; Day, V. W.; Francesconi, L. C.; Fredrich, M. F.; Klemperer, W. G.; Shum, W. *Inorg. Chem.* **1985**, *24*, 4055.
(21) Baldwin, J. E.; Reddy, V. P. *J. Am. Chem. Soc.* **1987**, *109*, 8051.

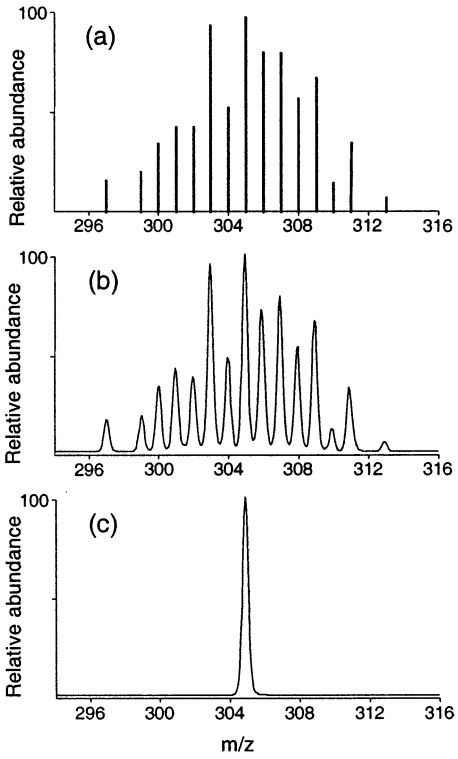

Figure 2. (a) Theoretical isotope pattern of $[Mo_2O_6(OH)]^-$; (b) Experimental isotope pattern of the ion assigned as $[Mo_2O_6(OH)]^-$; and (c) Mass selection of a single peak, *m*/*z* 305.

activation were carried out using standard isolation and excitation procedures[22] using the "advanced scan" function of the LCQ software.

Dimolybdate species display a distinctive isotope pattern (e.g., Figure 2a) due to the seven naturally occurring isotopes of molybdenum (^{92}Mo, 14.84; ^{94}Mo, 9.25; ^{95}Mo, 15.92; ^{96}Mo, 16.68; ^{97}Mo, 9.55; ^{98}Mo, 24.13; ^{100}Mo, 9.68 atom %). This facilitates assignment of ion stoichiometry via comparison of experimental and theoretical isotope patterns (e.g., Figure 2a, b). However, the broad isotope pattern can also make small mass changes difficult to detect (e.g. during isotope labeling experiments involving both hydrogen and deuterium). To avoid this problem, the *single* most intense peak was mass selected from the dimolybdate isotope manifold (e.g. Figure 2c), and used to follow the course of reactions. Quoted *m*/*z* values in the text refer to this most intense peak.

The instrument has been modified to permit introduction of neutral reagents into the ion trap, allowing the measurement of ion−molecule reaction rate constants.[23,24] The modifications and experimental procedure are described briefly. A known flow of helium (470−4880 cm^3/min) is passed through a stainless steel tube. A measured flow of neutral reagent (2.5−1000 μL/hour) is injected downstream into this tube from a gastight syringe using a Harvard syringe drive. The injection port is heated to about 50 °C to ensure rapid and efficient evaporation of neutral reagent into the helium flow. The composition of this external mixture is calculated using the known molar flow rates of helium and neutral reagent. A small fraction of this mixture (~0.25 mL/min) is carried through a restriction capillary into the ion trap, while the remainder is diverted to an exhaust system. The restriction capillary maintains the pressure of the ion trap at $P_b = 1.75 \pm 0.2 \times 10^{-3}$ Torr. Helium and neutral reagent molecules are able to exit the ion trap via effusion into the surrounding vacuum manifold. The lighter helium atoms effuse more quickly and are lost at a greater rate. The steady-state solution of the differential equation describing the molar flow of neutral reagents about the ion trap (i.e., the 'flux' of neutral reagents) allows the equilibrium pressure of neutral reagents, P_n (Torr), to be calculated (eq 8). Due to the large excess of neutral reagents relative to the reactant ion within the ion trap, all rates are measured under *pseudo* first-order conditions

$$P_n = P_b \times \frac{\text{molar flow rate of neutral}}{\text{molar flow rate of helium}} \times \sqrt{\frac{\text{molar mass of neutral}}{\text{molar mass of helium}}} \quad (8)$$

Rates were measured by varying the time delay between isolation of the reactant ion and its mass analysis ('Reaction Delay', RD). *Pseudo* first-order rates were estimated by extrapolation of plots of ln(reactant ion intensity) vs RD. 3−4 peaks from the isotope pattern of the reactant ion were mass selected and their decay monitored over at least 15 values of RD, spanning at least 3 reaction half-lives. The absolute intensity of the reactant ion was calculated by integration of its ion count within the mass selected window. Absolute rate constants were calculated by dividing the *pseudo* first order rate coefficient by the calculated concentration of neutral reagent in the ion trap. The absolute rate constants reported are the average of at least seven independent measurements conducted on at least 4 separate days. All rates are measured over at least a 5-fold neutral pressure range, using at least 3 different neutral reagent flowrates and 3 different helium flowrates. Upper bounds on rate constants for unreactive species were determined given that no reaction was observed after 10 s. Standard deviations in absolute rate constants were typically <10%. A conservative estimate of error is ±25%, but relative rates are expected to be more accurate due to cancellation of errors.

To test this procedure, experimental absolute rate constants determined for two reactions with the present instrumentation were compared with literature values obtained via flowing afterglow techniques at 298 K (eq 9,10).[25] This close agreement demonstrates that the present instrument provides ion−molecule rate constants of near thermal ions, consistent with previous rate measurements in a similar system[23] and findings that ions within the ion trap are essentially at room temperature[24]

$$Br^- + CH_3I \rightarrow CH_3Br + I^-$$

$$k_{lit} = 2.89 \times 10^{-11}\ \text{cm}^3\ \text{molecule}^{-1}\ \text{s}^{-1};\quad k_{exp} = 2.7 \times 10^{-11}\ \text{cm}^3\ \text{molecule}^{-1}\ \text{s}^{-1} \quad (9)$$

$$(CF_3)_2CHO^- + CH_3CH_2Br^- \rightarrow (CF_3)_2CHOH + CH_2CH_2 + Br^-$$

$$\rightarrow (CF_3)_2CHOCH_2CH_3 + Br^-$$

$$k_{lit} = 7.83 \times 10^{-12}\ \text{cm}^3\ \text{molecule}^{-1}\ \text{s}^{-1};\quad k_{exp} = 7.9 \times 10^{-12}\ \text{cm}^3\ \text{molecule}^{-1}\ \text{s}^{-1} \quad (10)$$

Reaction efficiencies (ϕ) were calculated by dividing the experimentally determined rate constant (k_{exp}) by theoretical predictions of ion−molecule collison rate constants[26] (k_{ado}); i.e., $\phi = k_{exp}/k_{ado}$. Uncertainties in reaction efficiencies have not been estimated, but would be comprised of uncertainties in the experimentally determined rate constant and in the theoretical collision rate constants. A complete list of experimental rate constants, theoretical collision rate constants and reaction efficiencies is included in the Supporting Information (Table S1).

The estimation of absolute collision energies applied during collisional activation experiments in quadrupole ion trap instruments is not straightforward. Colorado and Brodbelt have demonstrated a linear

(22) *Practical Aspects of Ion Trap Mass Spectrometry*; March, R. E., Todd, J. F. J., Eds.; CRC Press: Florida, 1995; (a) vol. 1 *Fundamentals of Ion Trap Mass Spectrometry*; (b) vol. 2 *Ion Trap Instrumentation*.
(23) (a) Flores, A. E.; Gronert, S. *J. Am. Chem. Soc.* **1999**, *121*, 2627. (b) Gronert, S.; Pratt, L. M.; Mogali, S. *J. Am. Chem. Soc.* **2001**, *123*, 3081.
(24) Gronert, S. *J. Am. Soc. Mass Spectrom.* **1998**, *9*, 845.
(25) Gronert, S.; DePuy, C. H.; Bierbaum, V. M. *J. Am. Chem. Soc.* **1991**, *113*, 4009.
(26) Su,T.; Bowers, M. T. In *Gas-Phase Ion Chemistry;* Bowers, M. T. Ed.; Academic Press: New York, 1979; p. 83.

relationship between the threshold activation voltage required for dissociation in ion-trap experiments and the established critical energies for a variety of ions.[27] However, separate calibration curves were required for hydrogen bonded and covalently bound species. The effect of factors such as ion mass and ion density, resonance excitation time and trapping well depth on threshold activation voltages in ion trap experiments have also been investigated.[28] A detailed investigation of these factors is beyond the scope of the present study, and we refrain from attempting quantification of critical energies of collisional activation reactions. However, to provide a qualitative insight into the critical energies of such reactions (e.g Figure 1, reaction 2), we have compared activation voltages required for these reactions with those required for the dissociation of two species with established critical energies, $Ag(CH_3OH)^+$ and $Fe(C_5H_5)_2^+$ (generated via ESI of $AgNO_3$ in CH_3OH and $Fe(C_5H_5)_2$ in CH_3CN, respectively).[29] These species were chosen as the activation voltages required for their dissociation effectively 'brackets' the activation voltages used in present experiments.

Threshold voltages were determined by mass selecting a single peak from the isotope pattern of the species of interest and applying an activation voltage for a period of 10 ms.[27] Activation voltages (V_{p-p}) were increased in a stepwise fashion until complete dissociation of the ion of interest was observed. In line with previous studies, the voltage at which the fragment ion intensity is 10% of the total ion intensity is defined as the 'threshold voltage'.[27] Given that relatively low concentrations of neutral reagents (typically $2-4 \times 10^{-7}$ Torr of CH_3OH or CH_3I) are required to generate species of interest, the effect of these neutral reagents on the collisional activation process was examined. No discernible effect in the measured threshold voltage was evident for either $Ag(CH_3OH)^+$ or $Fe(C_5H_5)_2^+$, suggesting the influence of low concentrations of neutral reagents on the measured 'threshold voltages' is negligible. Given important factors such as lifetime effects, kinetic shifts, differing excitation efficiencies and mass effects have been ignored in these experiments, the data presented is only intended as a rough approximation. Further, reactions described in the present work may exhibit reverse activation barriers, presenting a further complication to interpretation of data.

Theoretical Calculations. B3LYP Density Functional Theory (DFT) calculations[30] were performed using the GAMESS electronic structure program.[31] Local minima were characterized using numerical Hessians. The Effective Core Potential (ECP) basis sets of Stevens et al. were used for Cr, Mo, and W,[32] and the $6-311^{++}G^{**}$ basis set of Pople and co-workers for O and H.[33] Unscaled zero point energies are included for all species. Structures were visualized using MacMolPlt.[34] Cartesian coordinates and energies of optimized geometries are included in the Supporting Information (Figures S12, S14, S15).

Results and Discussion

Negative ion electrospray mass spectrometry of $(Bu_4N)_2[Mo_2O_7]$ in acetonitrile generated three major products: the dimolybdate dianion, $[Mo_2O_7]^{2-}$ (*m*/*z* 152), protonated dimolybdate, $[Mo_2O_6(OH)]^-$ (*m*/*z* 305; Figure 2), and the ion pair, $\{Bu_4N^+[Mo_2O_7]^{2-}\}^-$ (*m*/*z* 546).[35] Each of these species provided access to important intermediates in the catalytic cycles of Figure 1.

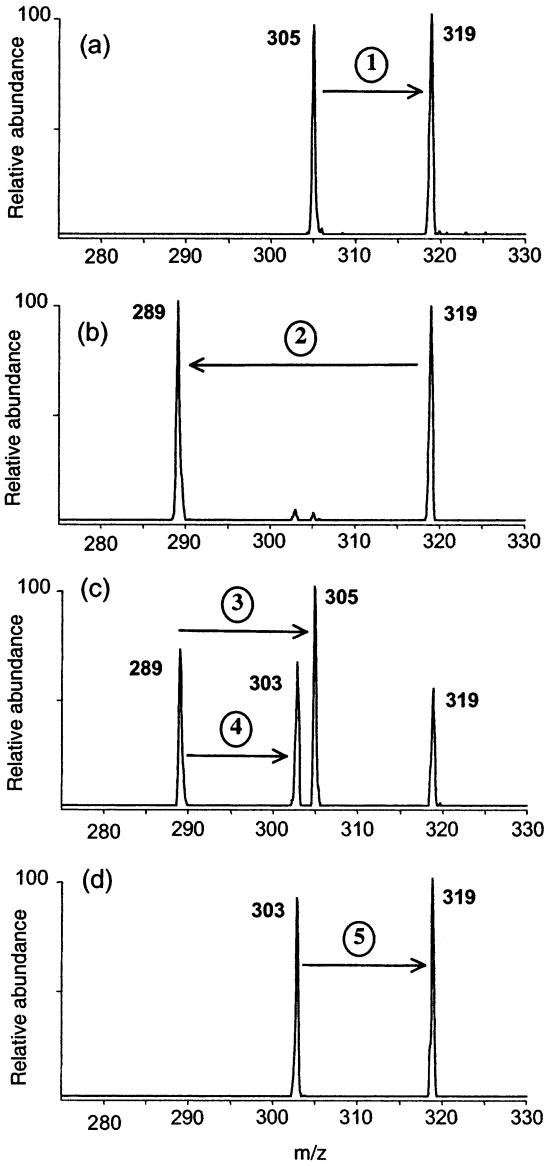

Figure 3. Mass spectra for reactions 1−5 of Cycles 1 and 2 (Figure 1). A single peak from the dimolybdate isotope manifold was mass selected and followed through each reaction. CH_3OH and CH_3NO_2 are present in the ion-trap in equal concentrations. (a) reaction 1 of Cycle 1; (b) reaction 2 of Cycles 1 and 2. The small peaks at *m*/*z* 303 and 305 are result of reaction 3 of Cycle 1 and reaction 4 of cycle 2 (see (c) below); (c) reaction 3 of Cycle 1 and reaction 4 of Cycle 2. This is the divergent point of the two cycles. The peak at *m*/*z* 319 is the result of the ions of *m*/*z* 303 and 305 reacting further (reactions 5, Cycle 2 and reaction 1, Cycle 1, respectively); and (d) reaction 5 of Cycle 2.

Catalytic Oxidation Of Alcohols by $[Mo_2O_6(OH)]^-$. The two catalytic cycles 1 and 2 of Figure 1 differ in the order of reaction of $[Mo_2O_5(OH)]^-$ with CH_3OH and CH_3NO_2. Representative mass spectra for reactions 1−5 of these cycles are included in Figure 3.

(27) Colorado, A.; Brodbelt, J. *J. Am. Soc. Mass Spectrom.* **1996**, *7*, 1116.
(28) (a) Jackson, G. P.; King, F. L.; Goeringer, D. E.; Duckworth, D. C. *Int. J. Mass Spectrom.* **2002**, *216*, 85. (b) Hart, K. J.; McLuckey, S. A. *J. Am. Soc. Mass Spectrom.* **1993**, *5*, 250.
(29) (a) $Ag(CH_3OH)^+ \rightarrow Ag^+ + CH_3OH$ see: El Aribi, H.; Shoeib, T.; Ling, Y.; Rodriquez, C. F.; Hopkinson, A. C.; Siu, K. W. M. *J. Phys. Chem. A* **2002**, *106*, 2908; and (b) $Fe(C_5H_5)_2^+ \rightarrow Fe(C_5H_5)^+ + C_5H_5^{\bullet}$ see: Faulk, J. D.; Dunbar, R. C. *J. Am. Chem. Soc.* **1992**, *114*, 8596.
(30) (a) Becke, A. D. *J. Chem. Phys.* **1993**, *98*, 1372. (b) Stephens, P. J.; Devlin, F. J.; Chabalowski, C. F.; Frisch, M. J. *J. Phys. Chem.* **1994**, *98*, 11 623.
(31) Schmidt, M. W.; Baldridge, K. K.; Boatz, J. A.; Elbert, S. T.; Gordon, M. S.; Jensen, J. H.; Koseki, S.; Matsunaga, N.; Nguyen, K. A.; Su, S. J.; Windus, T. L.; Dupuis, M.; Montgomery, J. A. *J. Comput. Chem.* **1993**, *14*, 1347.
(32) Stevens, W. J.; Krauss, M.; Basch, H.; Jasien, P. G.; *Can. J. Chem.* **1992**, *70*, 612.
(33) Krishnan, R.; Binkley, J. S.; Seegar, R.; Pople, J. A. *J. Chem. Phys.* **1980**, *72*, 650.
(34) Bode, B. M.; Gordon, M. S. *J. Mol. Graphics Mod.* **1998**, *16*, 133.
(35) ESI of $(Bu_4N)_2[Mo_2O_7]$ has been reported previously: from CH_3CN (a) Lau, T.-C.; Wang, J.; Guevremont, R.; Siu, K. W. M. *Chem. Commun.* **1995**, 877; and from CH_3OH. (b) Takara, S.; Ogo, S.; Watanabe, Y.; Nishikawa, K.; Kinoshita, I.; Isobe, K. *Angew. Chem., Int. Ed. Engl.* **1999**, *38*, 3051.

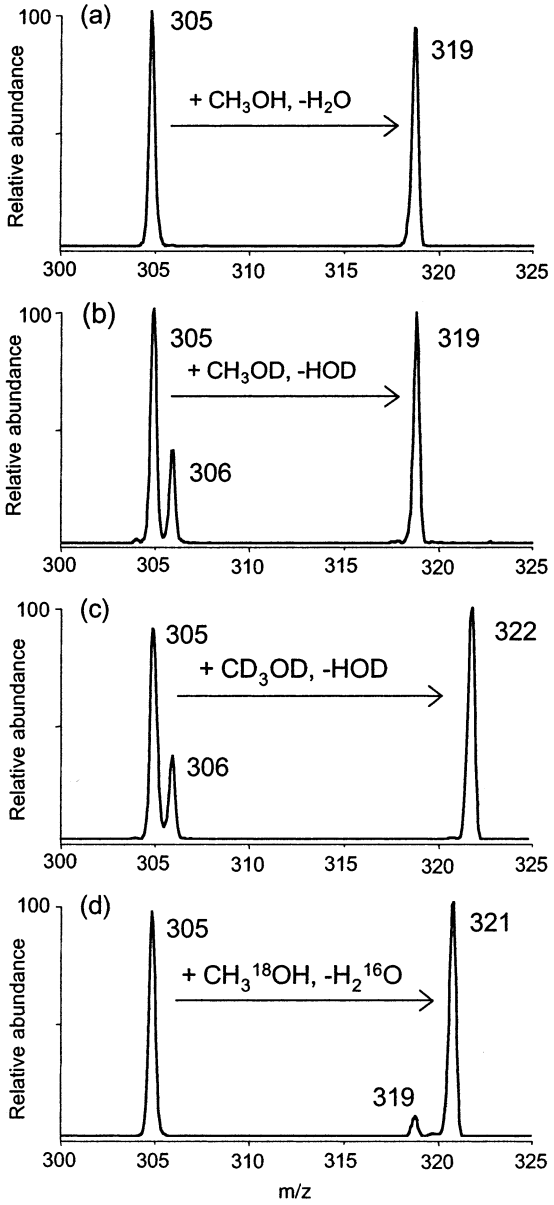

Figure 4. Mass spectra showing the reaction of $[Mo_2O_6(OH)]^-$ with isotopically labeled methanol. Reaction of $[Mo_2O_6(OH)]^-$ (*m*/*z* 305) with the following: (a) CH_3OH to form $[Mo_2O_6(OCH_3)]^-$ (*m*/*z* 319); (b) CH_3OD to form $[Mo_2O_6(OCH_3)]^-$ (*m*/*z* 319). Note that H/D exchange with CH_3OD also occurs to form $[Mo_2O_6(OD)]^-$ (*m*/*z* 306); (c) CD_3OD to form $[Mo_2O_6(OCD_3)]^-$ (*m*/*z* 322). Note that H/D exchange occurrs again; and (d) $CH_3{}^{18}OH$ to form $[Mo_2O_6(^{18}OCH_3)]^-$ (*m*/*z* 321). The peak at *m*/*z* 319 is a result of reaction with $CH_3{}^{16}OH$ impurity in the $CH_3{}^{18}OH$ sample.

In cycle 1, $[M^{VI}{}_2O_6(OH)]^-$ (*m*/*z* 305) reacted with methanol to form $[Mo^{VI}{}_2O_6(OCH_3)]^-$ (*m*/*z* 319) and eliminate water (Figure 1, reaction 1; Figure 3a). Collisional activation of $[Mo^{VI}{}_2O_6(OCH_3)]^-$ eliminated formaldehyde with the formation of 2e$^-$-reduced $[Mo^{V}{}_2O_5(OH)]^-$ (*m*/*z* 289) (reaction 2; Figure 3b). This ion then underwent an oxygen atom transfer reaction with nitromethane to regenerate $[Mo^{VI}{}_2O_6(OH)]^-$ and complete cycle 1 (reaction 3; Figure 3c).

Reaction 2 is common to both cycles. Its product, $[Mo^{V}{}_2O_5(OH)]^-$ (*m*/*z* 289), reacted with either CH_3NO_2 (cycle 1, reaction 3) or with CH_3OH (cycle 2, reaction 4). This is the divergent point of the two cycles. Reaction with CH_3OH (cycle 2, reaction 4; Figure 3c) produced $[Mo^{V}{}_2O_5(OCH_3)]^-$ (*m*/*z* 303). This ion

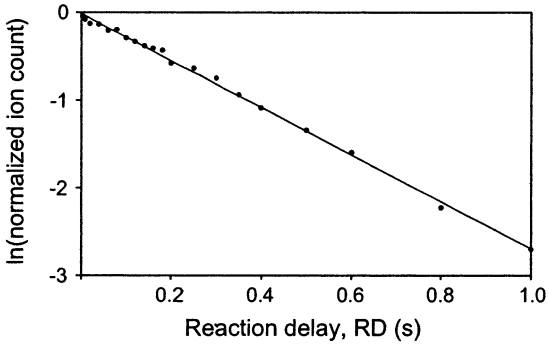

Figure 5. First-order plot for reaction of $[Mo_2O_6(OH)]^-$ with CH_3OH (Figure 1, reaction 1).

then reacted with CH_3NO_2 to generate $[Mo^{VI}{}_2O_6(OCH_3)]^-$ (*m*/*z* 319) and complete cycle 2 (reaction 5, Figure 3d).

The multistage trapping capabilities of the ion-trap instrument allowed cycles 1 and 2 to be completed thrice and twice, respectively, on the same population of ions. This confirmed that they were truly catalytic for the oxidation of primary and secondary alcohols to aldehydes (Figures S2, S3). Individual reactions are now discussed in more detail using the numbering system shown in Figure 1.

Cycle 1, Reaction 1: Interaction of $[Mo_2O_6(OH)]^-$ with Alcohols. Mass selection of $[Mo_2O_6(OH)]^-$ (*m*/*z* 305) in the presence of methanol solely led to the formation of a new ion, *m*/*z* 319, assigned as $[Mo_2O_6(OCH_3)]^-$ (eq 1a). Isotope labeling experiments were consistent with the binding of methoxo ligand from methanol and the elimination of hydroxo ligand as neutral water (eq 1a−d, Figure 4). Competitive H/D exchange was also observed for reaction with CH_3OD and CD_3OD (Figure 4). Reaction with methanol followed smooth *pseudo* first-order kinetics (Figure 5**)** with a reaction efficiency of approximately 5% ($\phi = 0.049$, Table 1)

$$[Mo_2O_6(OH)]^- (m/z\ 305) + CH_3OH \rightarrow [Mo_2O_6(OCH_3)]^- (319) + H_2O \quad (1a)$$

$$[Mo_2O_6(OH)]^- (305) + CH_3OD \rightarrow [Mo_2O_6(OCH_3)]^- (319) + DOH \quad (1b)$$

$$[Mo_2O_6(OH)]^- (305) + CD_3OD \rightarrow [Mo_2O_6(OCD_3)]^- (322) + DOH \quad (1c)$$

$$[Mo_2{}^{16}O_6(^{16}OH)]^- (305) + CH_3{}^{18}OH \rightarrow [Mo_2{}^{16}O_6(^{18}OCH_3)]^- (321) + H_2{}^{16}O \quad (1d)$$

A reaction between $[Mo_2O_7]^{2-}$ and CH_3OH to produce $[Mo_2O_6(OCH_3)]^-$ was reported incorrectly in our previous communication.[8] In fact, $[Mo_2O_7]^{2-}$ is unreactive toward CH_3OH. In those experiments, an acetic acid impurity in the gas handling system resulted in protonation of the dianion to form $[Mo_2O_6(OH)]^-$, which then reacted with CH_3OH to form $[Mo_2O_6(OCH_3)]^-$ (equivalent to reaction 1).

$[Mo_2O_6(OH)]^-$ also reacted with other alcohols to from alkylated dimolybdate anions $[Mo_2O_6(OR)]^-$ (Table 1, Fig. S4).[36] A comparison of reaction efficiency and alcohol acidity for primary alcohols suggests an approximate direct dependence, consistent with a mechanism involving deprotonation of the

Table 1. Reaction Rates for the Reaction of $[Mo_2O_6(OH)]^-$ with Alcohols

alcohol	ΔG°_{acid}[a] (kcal/mol)	k_{exp}[b]	reaction efficiency, ϕ[c]
CH_3OH	375.1	6.9	0.049
CH_3CH_2OH	371.7	9.1	0.070
$CH_3CH_2CH_2OH$	369.6	14	0.11
$(CH_3)_2CHOH$	368.5	8.9	0.069
$(CH_3)_3COH$	368.1	2.8	0.023
CFH_2CH_2OH[d]	364.6	25	n/a
CF_3CH_2OH[d]	354.1	66	n/a

[a] Gas-phase acidity is defined as the Gibbs energy change for the reaction $ROH \rightarrow RO^- + H^+$.[37] [b] $\times 10^{-11}$ cm^3 molecules^{-1} s^{-1}. [c] $\phi = k_{exp}/k_{ADO}$. [d] Theoretical collision rate constants and thus reaction efficiencies for these alcohols have not been calculated as their dipole moments have not been determined experimentally.

alcohol and binding of the alkoxo ligand, as indicated by the isotope labeling experiments (eq 1a−d). The branched alcohols reacted more slowly than expected based on their acidity, presumably due to steric constraints. Because the presence of alcohol in the ion-trap can interfere with studies of subsequent steps of the catalytic cycles (e.g., Figure 1, Figure 3c; reaction 4 of cycle 2 competes with reaction 3 of cycle 1), an independent method of generating $[Mo_2O_6(OR)]^-$ is now discussed.[38]

Formation of $[Mo_2O_6(OBu)]^-$ from the Ion-Pair, $\{Bu_4N^+$-$[Mo_2O_7]^{2-}\}^-$. Collisional activation of $\{Bu_4N^+[Mo_2O_7]^{2-}\}^-$ resulted in elimination of neutral tri-*n*-butylamine, NBu_3, and formation of $[Mo_2O_6(OBu)]^-$ (*m*/*z* 361) (eq 11). This reaction is proposed to occur via an S_N2 pathway: the nucleophilic dimolybdate dianion attacks the α-carbon of the tetrabutylammonium cation. Related S_N2 reactions within ion-pairs containing organo dianions are known.[39] Interestingly, S_N2 O-alkylation of larger polyoxometalate anions via reaction with strongly electrophilic trialkyloxonium ions have also been observed in condensed phases (eqs 12,13)[40]

$$\{Bu_4N^+[Mo_2O_7]^{2-}\}^- \rightarrow [Mo_2O_6(OBu)]^- + NBu_3 \quad \text{gas phase} \quad (11)$$

$$[PMo_{12}O_{40}]^{3-} + (CH_3)_3O^+ \rightarrow [PMo_{12}O_{39}(OCH_3)]^{2-} + (CH_3)_2O \quad \text{solution} \quad (12)$$

$$(R_3O)_3[PW_{12}O_{40}] \rightarrow (R_3O)_2[PW_{12}O_{39}(OR)]^{2-} + R_2O \quad \text{solid state} \quad (13)$$

The presence of a butoxo ligand in the product of eq 11 was indicated by the ligand switching reaction with methanol (eq 14). Results from reaction of $[Mo_2O_6(OBu)]^-$ with labeled methanol (Figure S5) were equivalent to those for $[Mo_2O_6(OH)]^-$ (eq 1a−d), suggesting a similar mechanism of reaction and consistent with elimination of the butoxo ligand as butanol. Reaction efficiency for this reaction was 1.7% ($\phi = 0.017$), about one-third of that observed for reaction of $[Mo_2O_6(OH)]^-$ with methanol (Table 1). $[Mo_2O_6(OBu)]^-$ also underwent analogous ligand switching reactions with other alcohols (Figure S6)

$$[Mo_2O_6(OBu)]^- (m/z\ 361) + CH_3OH \rightarrow [Mo_2O_6(OCH_3)]^- (319) + BuOH \quad (14)$$

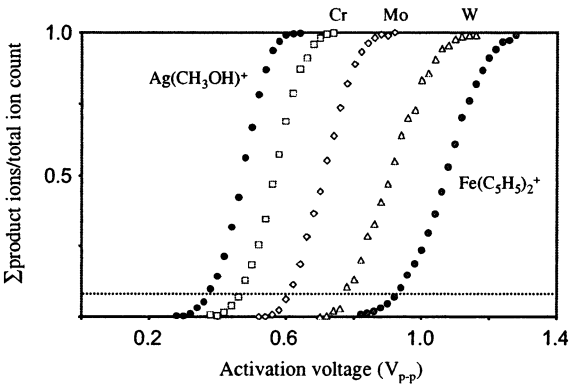

Figure 6. Plot of Reaction Extent (Σproduct ions/total ion count) vs activation voltage (V_{p-p}) for elimination of H_2CO from $[M_2O_6(OCH_3)]^-$ (M = Cr, Mo, W). The critical energies for dissociation of $Ag(CH_3OH)^+$ (33.0 ± 3.7 kcal/mol) and $Fe(C_5H_5)_2^+$ (85 ± 7 kcal/mol) are known.[29] The dashed line corresponds to 10% reaction extent, the point at which threshold activation voltages are measured.

Cycles 1 and 2, Reaction 2: Elimination of Formaldehyde from $[Mo^{VI}_2O_6(OCH_3)]^-$. Collisional activation of $[Mo^{VI}_2O_6$-$(OCH_3)]^-$ (*m*/*z* 319) resulted in a mass loss of 30, consistent with elimination of neutral formaldehyde (Figure 1, reaction 2; Figure 3b). The product ion of this reaction, of stoichiometry $[Mo_2, O_6, H]^-$ (*m*/*z* 289), is tentatively assigned as $[Mo^{V}_2O_5$-$(OH)]^-$. The mechanism of reaction was investigated via isotopically labeled methoxo ligands generated via eq 1a−d (eq 2a−c, Figure S7). These experiments demonstrated that formaldehyde originated from the methoxo ligand. The dimolybdate center retained the two electrons and proton produced in the formal redox half-equation: $CH_3O^- \rightarrow H_2CO + 2e^- + H^+$

$$[Mo^{VI}_2O_6(OCH_3)]^- (m/z\ 319) \rightarrow [Mo^{V}_2O_5(OH)]^- (289) + H_2CO \quad (2a)$$

$$[Mo^{VI}_2O_6(OCD_3)]^- (322) \rightarrow [Mo^{V}_2O_5(OD)]^- (290) + D_2CO \quad (2b)$$

$$[Mo^{VI}_2{}^{16}O_6(^{18}OCH_3)]^- (321) \rightarrow [Mo^{V}_2{}^{16}O_5(^{16}OH)]^- (289) + H_2C^{18}O \quad (2c)$$

An estimate of the critical energy of reaction 2 was derived via comparison with species of known critical energies (Figure 6). The critical energy for dissociation of $Ag(CH_3OH)^+$ is 33.0 ± 3.7 kcal/mol (threshold voltage = 0.38 V_{p-p}), and the critical energy for dissociation of $Fe(C_5H_5)_2^+$ is 85 ± 7 kcal/mol (threshold voltage = 0.94 V_{p-p}).[29] The threshold voltages for these reactions bracket the threshold voltage observed for $[Mo_2O_6(OCH_3)]^-$ (threshold voltage = 0.61 V_{p-p}, Figure 6). This suggests a crude estimate of 55 ± 20 kcal/mol for the critical energy of reaction 2.

(36) For examples of condensation of alcohols at M-OH bonds in the gas-phase, see: (a) Fiedler, A.; Schröder, D.; Schwarz, H.; Tjelta, B. L.; Armentrout, P. B. *J. Am. Chem. Soc.* **1996**, *118*, 5047. (b) Richardson, D. E.; Lang, G. H. L.; Crestoni, E.; Ryan, M. F.; Eyler, J. E. *Int. J. Mass Spectrom.* **2001**, *204*, 255. (c) Jackson, P.; Fisher, K. J.; Willett, G. D. *Chem. Phys.* **2000**, *262*, 179.
(37) Alcohol acidities are from: http://webbook.nist.gov/chemistry/.
(38) Alcohol is present in the ion trap during all stages of a multistage experiment. If alcohol is used in initial reactions of the catalytic cycle (e.g., reaction 1) it remains present during later reactions.
(39) Gronert, S.; Azebu, J. *Org. Lett.* **1999**, *1*, 503.
(40) (a) Knoth, W. H.; Harlow, R. L. *J. Am. Chem. Soc.* **1981**, *103*, 4265. (b) Knoth, W. H.; Farlee, R. D. *Inorg. Chem.* **1984**, *23*, 4765.

Dimolybdate anions with a range of deuterated ethoxo ligands were synthesized by reaction of $[Mo_2O_6(OH)]^-$ with the appropriately labeled ethanol. Collisional activation of these species resulted in elimination of the ethoxo ligand as acetaldehyde (eq 15a−c, Figure 7).[41] The hydrogen retained on the dimolybdate center originated from the α-position of the alkoxo ligand only (Figure 7a,b). These results are consistent with a mechanism involving transfer of an hydrogen atom from the α-position, reduction of the binuclear metal center and elimination of aldehyde, i.e., consistent with the *Westheimer* mechanism.[42] This mechanism was originally proposed to account for the elimination of aldehyde from chromate-ester intermediates in the oxidation of alcohols by high valent chromium(VI)-oxo reagents

$$[Mo^{VI}{}_2O_6(OCH_2CH_3)]^- (m/z\ 333) \rightarrow [Mo^{V}{}_2O_5(OH)]^- (289) + CH_3CHO \quad (15a)$$

$$[Mo^{VI}{}_2O_6(OCD_2CH_3)]^- (335) \rightarrow [Mo^{V}{}_2O_5(OD)]^- (290) + CH_3CDO \quad (15b)$$

$$[Mo^{VI}{}_2O_6(OCH_2CD_3)]^- (336) \rightarrow [Mo^{V}{}_2O_5(OH)]^- (289) + CD_3CHO \quad (15c)$$

Acetaldehyde elimination from $[Mo_2O_6(OCHDCH_3)]^-$ was examined using the ion synthesized via reaction of $[Mo_2O_6(OH)]^-$ with CH_3CHDOH. Collisional activation resulted in the loss of a mixture of CH_3CDO and CH_3CHO (eq 15d,e; Figure 7c). The product ratio of CH_3CDO to CH_3CHO (inferred from the relative ion intensities of the product anions) suggeted a kinetic isotope effect of approximately 1.9 ± 0.4 for this reaction under the collisional activation conditions of the present experiments[43]

$$[Mo^{VI}{}_2O_6(OCHDCH_3)]^- (m/z\ 334) \rightarrow [Mo^{V}{}_2O_5(OH)]^- (289) + CH_3CDO \approx 65\% \quad (15d)$$

$$\rightarrow [Mo^{V}{}_2O_5(OD)]^- (290) + CH_3CHO \approx 35\% \quad (15e)$$

Collisional activation of dimolybdate centers with branched alkoxo ligands was also examined (eq 17, 19) and compared with their straight chain counterparts (eq 16, 18, Figure S8). These species were synthesized via reaction of $[Mo_2O_6(OH)]^-$ with the appropriate alcohol, whereas $[Mo_2O_6(O^nBu)]^-$ was generated from $\{Bu_4N^+[Mo_2O_7]^{2-}\}^-$ (eq 11). Collisional activation of dimolybdate centers with straight chain alkoxo ligands results in elimination of the corresponding aldehyde (eq 16, 18).[41] In contrast, collisional activation of $[Mo_2O_6(OC(CH_3)_3]^-$ eliminated 2-methyl-propene (eq 19). The redox mechanism has been switched off by the absence of α-hydrogen in the tertiary alkoxo ligand. The observed products are consistent with transfer of a β-hydrogen atom from the ^{t}Bu substituent to an oxo ligand of the dimolybdate center and elimination of 2-methyl-propene. Collisional activation of $[Mo_2O_6(OCH(CH_3)_2]^-$ resulted in elimination of both acetone and propene (eq 17a,b). This is consistent with an increased barrier to aldehyde elimination due to increased steric bulk at the α-carbon of the secondary alkyl group

$$[Mo^{VI}{}_2O_6(OCH_2CH_2CH_3)]^- \rightarrow [Mo^{V}{}_2O_5(OH)]^- + CH_3CH_2CHO \quad (16)$$

$$[Mo^{VI}{}_2O_6(OCH(CH_3))_2]^- \rightarrow [Mo^{V}{}_2O_5(OH)]^- + (CH_3)_2CO \approx 75\% \quad (17a)$$

$$\rightarrow [Mo^{VI}{}_2O_6(OH)]^- + CH_3CH{=}CH_2 \approx 25\% \quad (17b)$$

$$[Mo^{VI}{}_2O_6(OCH_2(CH_2)_2CH_3)]^- \rightarrow [Mo^{V}{}_2O_5(OH)]^- + CH_3(CH_2)_2CHO \quad (18)$$

$$[Mo^{VI}{}_2O_6(OC(CH_3)_3)]^- \rightarrow [Mo^{VI}{}_2O_6(OH)]^- + (CH_3)_2C{=}CH_2 \quad (19)$$

The elimination of aldehyde from $[Mo_2O_6(OCHR_2)]^-$ species (reaction 2, eq 2, 15−18) does not proceed without the use of collisional activation. This reaction represents the rate-limiting step in the gas-phase catalytic cycles of Figure 1.

Cycle 1, Reaction 3: Interaction of $[Mo^{V}{}_2O_5(OH)]^-$ with CH_3NO_2. The product of reaction 2 was assigned to $[Mo^{V}{}_2O_5(OH)]^-$ whose stoichiometry differs from $[Mo^{VI}{}_2O_6(OH)]^-$ by an oxygen atom. This suggested closing cycle 1 by an oxygen atom transfer reaction. The reaction of $[Mo^{V}{}_2O_5(OH)]^-$ with potential oxygen atom transfer reagents CH_3NO_2, $(CH_3)_2SO$, N_2O, O_2, and 1,2-epoxybutane was investigated. To avoid competing reactions with alcohols,[38] $[Mo_2O_5(OH)]^-$ was generated in a sequence of reactions from the ion-pair (eqs 11 and 18). Only CH_3NO_2 reacted with $[Mo_2O_5(OH)]^-$ via oxygen atom transfer. [44,45]

Mass selection of $[Mo^{V}{}_2O_5(OH)]^-$ (*m*/*z* 289) and reaction with nitromethane solely resulted in the formation of a new ion at *m*/*z* 305, assigned to $[Mo^{VI}{}_2O_6(OH)]^-$ (eq 3; Figure 1, reaction 3; Figure 3c). This reaction deviated from smooth first order kinetics (Figure 8a), with approximately 20% of the sample being unreactive.[46] A theoretical decay curve could be fitted using an experimental estimate of the amount of unreactive

(41) A very small amount of alkene loss is also observed from dimolybdate centres with straight chain alkoxo ligands. This typically represents less than 2% of the amount of aldehyde loss.

(42) Westheimer, F. H. *Chem. Rev.* **1949**, *45*, 419. We adopt the notation whereby the first carbon of the alkoxo ligand is denoted as the α-carbon.

(43) This kinetic isotope effect (KIE) is estimated based on experiments where the activation voltage, activation time and, thus, reaction extent were systematically varied. The estimate of 1.9 ± 0.4 represents an average value under conditions where greater than 20% reaction occurred, and the error in this estimate is based upon the upper and lower experimental values obtained under these conditions. Given that this reaction only occurs upon collisional activation, and that the ions in these experiments are significantly above room temperature, the KIE at 298 K may be larger. A crude estimate of the KIE effect for β-hydrogen transfer and ethene elimination can also be inferred from these experiments: this channel represents 2.3% of products for $[Mo_2O_6(OCH_2CH_3)]^-$ and 0.4% for $[Mo_2O_6(OCH_2CD_3)]^-$, suggesting a crude estimate for the KIE of this reaction of 6.

(44) Upper bounds can be placed on the rate constants for reaction of $[Mo^{V}{}_2O_5(OH)]^-$ with these unreactive neutrals: $(CH_3)_2SO$, $k_{exp} < 5 \times 10^{-14}$ cm^3 molecule^{-1} s^{-1}; 1,2-epoxybutane, $k_{exp} < 5 \times 10^{-14}$ cm^3 molecule^{-1} s^{-1}; N_2O, $k_{exp} < 5 \times 10^{-13}$ cm^3 molecule^{-1} s^{-1}. There appears to be no correlation between the enthalpy of oxo transfer for these neutrals (Holm, R. H.; Donahue, J. P. *Polyhedron*, **1993**, *12*, 571) and their reactivity towards $[Mo^{V}{}_2O_5(OH)]^-$. This suggests kinetic factors are important.

(45) The reactivity of O_2 towards $[Mo^{V}{}_2O_5(OH)]^-$ is of particular interest given that this is the oxidant used in the industrial process (eq 7). Reaction of $[Mo^{V}{}_2O_5(OH)]^-$ (*m*/*z* 289) with dioxygen proceeded slowly ($\phi \approx 0.004$), forming a product at *m*/*z* 321, assigned to the ion−molecule complex $[Mo^{V}{}_2O_5(OH){-}O_2]^-$. This ion could not be mass selected in the ion trap instrument, presumably due to its 'fragile' nature (consistent with the observation of 'peak fronting' for this species, see: McClellan, J. E.; Murphy, J. P., III.; Mulholland, J. J.; Yost, R. A. *Anal. Chem.* **2002**, *74*, 402).

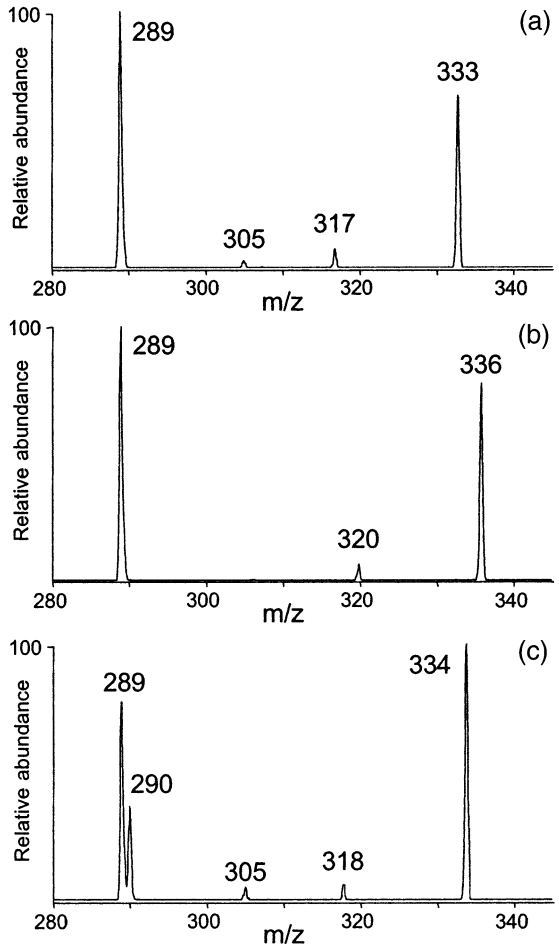

Figure 7. Collisional activation of selectively deuterated $[Mo_2O_6(OCH_2CH_3)]^-$ centers. Identical collisional activation conditions were used in each experiment. (a) Collisional activation of $[Mo_2O_6(OCH_2CH_3)]^-$ (*m*/*z* 333) to eliminate CH_3CHO and form $[Mo_2O_5(OH)]^-$ (*m*/*z* 289). The peak at *m*/*z* 305 is the product of elimination of CH_2CH_2 to form $[Mo_2O_6(OH)]^-$, whereas the peak at *m*/*z* 317 is the product of reaction of *m*/*z* 289 with CH_3CH_2OH. (b) Collisional activation of $[Mo_2O_6(OCH_2CD_3)]^-$ (*m*/*z* 336) to eliminate CD_3CHO and form $[Mo_2O_5(OH)]^-$ (*m*/*z* 289). The peak at *m*/*z* 320 is the product of reaction of *m*/*z* 289 with CD_3CH_2OH. (c) Collisional activation of $[Mo_2O_6(OCHDCH_3)]^-$ (*m*/*z* 334) to eliminate CH_3CDO or CH_3CHO and form $[Mo_2O_5(OH)]^-$ (*m*/*z* 289) or $[Mo_2O_5(OD)]^-$ (*m*/*z* 290), respectively. The peak at *m*/*z* 305 is the product of elimination of $CHDCH_2$ to form $[Mo_2O_6(OH)]^-$, whereas the peak at *m*/*z* 318 the product of reaction of *m*/*z* 289 and *m*/*z* 290 with CH_3CHDOH.

component, together with the experimentally determined rate constant, k_{exp} (Figure 8a). This reaction occurred at 70% of the collision rate ($\phi = 0.70$). The apparent presence of an unreactive form is discussed in more detail later

$$[Mo^{V}{}_2O_5(OH)]^- + CH_3NO_2 \rightarrow [Mo^{VI}{}_2O_6(OH)]^- + CH_3NO \quad (3)$$

Reaction 3 closes cycle 1 (Figure 1). Using the multistage trapping capabilities of the ion trap instrument it has been possible to carry out the complete cycle 1 three times on the same population of ions (Fig. S2). This establishes cycle 1 as truly catalytic for the oxidation of primary and secondary alcohols to aldehydes and ketones, respectively.

Cycle 2, Reaction 4: Interaction of $[Mo_2O_5(OH)]^-$ with Methanol. $[Mo^{V}{}_2O_5(OH)]^-$ is formulated to contain an hydroxo ligand, and so its reactivity toward alcohol was of interest. Mass selection of $[Mo^{V}{}_2O_5(OH)]^-$ (*m*/*z* 289) and reaction with

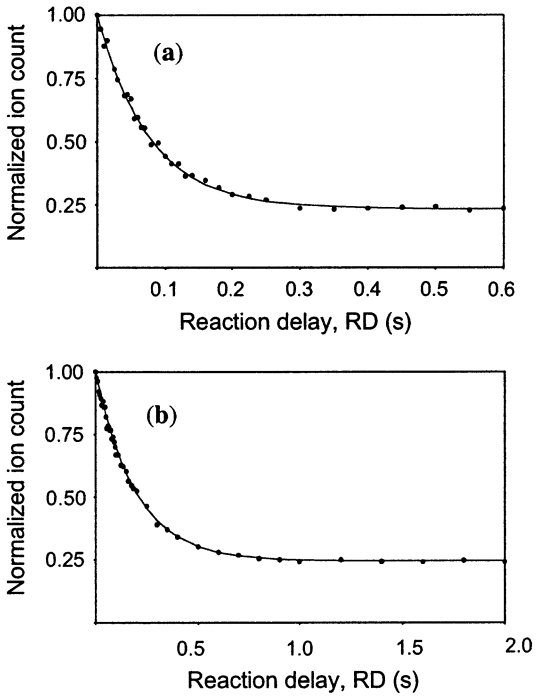

Figure 8. Reaction of $[Mo_2O_5(OH)]^-$ with **(a)** CH_3NO_2 (filled circles) and **(b)** CH_3OH (filled circles). Note the deviation from pesudo first order kinetics in both plots: approximately 20% of the total ion count is unreactive toward both these neutral reagents. The solid lines represent theoretical fits based on the experimentally determined rate constant and amount of unreactive component.

methanol leads to the formation of a new ion at *m*/*z* 303, assigned to $[Mo^{V}{}_2O_5(OCH_3)]^-$ (Figure 1, cycle 2, reaction 4; Figure 3c). Isotope labeling experiments were consistent with binding of methoxo ligand from methanol and elimination of hydroxo ligand as neutral water (eq 4a−d, Fig. S9). These results mirror those observed for reaction of $[Mo^{VI}{}_2O_6(OH)]^-$ with methanol (eq 1a−d), suggesting similar mechanisms of reaction and supporting the presence of ligand hydroxo in both species

$$[Mo^{V}{}_2O_5(OH)]^- (m/z\ 289) + CH_3OH \rightarrow [Mo^{V}{}_2O_5(OCH_3)]^- (303) + H_2O \quad (4a)$$

$$[Mo^{V}{}_2O_5(OH)]^- (289) + CH_3OD \rightarrow [Mo^{V}{}_2O_5(OCH_3)]^- (303) + DOH \quad (4b)$$

$$[Mo^{V}{}_2O_5(OH)]^- (289) + CD_3OD \rightarrow [Mo^{V}{}_2O_5(OCD_3)]^- (306) + DOH \quad (4c)$$

$$[Mo^{V}{}_2{}^{16}O_5(^{16}OH)]^- (289) + CH_3{}^{18}OH \rightarrow [Mo^{V}{}_2{}^{16}O_5(^{18}OCH_3)]^- (305) + H_2{}^{16}O \quad (4d)$$

$[Mo_2O_5(OH)]^-$ (generated via the sequence eqs 11 and 18) reacted rapidly with methanol (Figure 8b). Deviation from smooth first-order kinetics was again evident and the qualitative observations are similar to those for reaction of this ion with nitromethane, i.e., 20% was unreactive (Figure 8a).[46] After correction for this unreactive component, smooth first-order

(46) An upper bound can be placed on the rate constant for reaction of the unreactive component of $[Mo_2, O_6, H]^-$ with nitromethane and methanol: $k_{exp} < 5 \times 10^{-14}$ cm^3 molecule^{-1} s^{-1}.

kinetics were observed for at least 4 half-lives, with the reaction occurring at the collision rate ($\phi = 1.0$).

While the mechanisms of reaction of $[Mo^{VI}_2O_6(OH)]^-$ and $[Mo^{V}_2O_5(OH)]^-$ with methanol seemed similar, the rates of reaction differed markedly: $[Mo^{VI}_2O_6(OH)]^-$ reacted at only 5% of the collision rate ($\phi = 0.049$), whereas the reactive component of $[Mo^{V}_2O_5(OH)]^-$ reacted at the collision rate ($\phi = 1.0$). The increased reactivity of $[Mo^{V}_2O_5(OH)]^-$ can be attributed to (i) reduced coordinative saturation and/or (ii) increased basicity of the hydroxo ligand due to the lower oxidation level of the binuclear center (weaker acid). $[Mo^{V}_2O_5(OH)]^-$ also reacted with other alcohols ROH in an analogous reaction to form $[Mo_2O_5(OR)]^-$ and eliminate neutral water (Figure S10).

The product ion from reaction of $[Mo^{V}_2O_5(OH)]^-$ with alcohol, $[Mo^{V}_2O_5(OR)]^-$, differs in stoichiometry from $[Mo^{VI}_2O_6(OR)]^-$ by an oxygen atom. This suggested comparison of the behavior of these ions upon collisional activation. The competition between aldehyde and alkene elimination from $[Mo^{VI}_2O_6(OR)]^-$ was described above (eqs 2, 15−19). A dramatic difference in reactivity is observed for $[Mo^{V}_2O_5(OR)]^-$, which undergoes heterolytic cleavage of the O−R bond of the alkoxo ligand and elimination of an alkyl radical (eq 20, Figure S11).[47] The inability of $[Mo^{V}_2O_5(OR)]^-$ to eliminate aldehyde reinforces the importance of the stronger oxidizing power of the dimolybdate(VI) center

$$[Mo_2O_5(OR)]^- \rightarrow [Mo_2O_6]^- + R^\bullet \qquad (20)$$

Cycle 2, Reaction 5: Reaction of $[Mo^{V}_2O_5(OCH_3)]^-$ with CH_3NO_2. Mass selection of $[Mo^{V}_2O_5(OCH_3)]^-$ (*m*/*z* 303) and reaction with nitromethane resulted in formation of a new product ion with a mass increase of 16 Da, assigned as $[Mo^{VI}_2O_6(OCH_3)]^-$ (*m*/*z* 319) (eq 5, Figure 1, Cycle 2, reaction 5; Figure 3d). This reaction proceeded at 61% of collision rate ($\phi = 0.61$). This rate can be compared with that for reaction of $[Mo^{V}_2O_5(OH)]^-$ with CH_3NO_2 (eq 4; $\phi = 0.70$). The slight decrease in rate for $[Mo^{V}_2O_5(OCH_3)]^-$ may arise from the greater steric demands of the methoxo ligand relative to an hydroxo ligand. In contrast with $[Mo^{V}_2O_5(OH)]^-$ (Figure 8a), $[Mo^{V}_2O_5(OCH_3)]^-$ reacted with nitromethane under smooth *pseudo* first-order kinetics. This is consistent with the reactive component only of $[Mo^{V}_2O_5(OH)]^-$ reacting with methanol to form $[Mo^{V}_2O_5(OCH_3)]^-$ in reaction 4 of cycle 2

$$[Mo^{V}_2O_5(OCH_3)]^- (m/z\ 303) + CH_3NO_2 \rightarrow [Mo^{VI}_2O_6(OCH_3)]^- (319) + CH_3NO \qquad (5)$$

Reaction 5 closes cycle 2 (Figure 1). Using the multistage trapping capabilities of the ion trap instrument it has been possible to carry out the complete cycle 2 twice on the same population of ions (Figure S3). This establishes cycle 2 as truly catalytic for the oxidation of primary and secondary alcohols to aldehydes and ketones, respectively.[48]

Nature of the Unreactive Component of $[Mo_2O_5(OH)]^-$. Approximately 20% of the sample assigned to $[Mo^{V}_2O_5(OH)]^-$ did not react with either nitromethane or methanol on the time scale and concentrations of the experiments (Figure 8a,b; reactions 3, 4). This could be due to the presence of (i) excited 'hot' ions, of greater reactivity relative to ground-state ions, or (ii) isomers of differing reactivity.

Given that the ion assigned to $[Mo^{V}_2O_5(OH)]^-$ was synthesized via collisional activation of $[Mo^{VI}_2O_6(OBu)]^-$ (eq 11, 18), the generation of 'hot' ions was a possibility. However, the high background pressure of helium within the ion trap relative to the pressure of reactive neutrals ensured that ions underwent a large number of thermalizing collisions with helium before collision with reactive neutrals.[49] This suggested that the presence of 'hot' ions is an unlikely explanation for the unusual reactivity of the $[Mo^{V}_2O_5(OH)]^-$ sample. The presence of isomeric forms generated by competitive mechanisms of aldehyde elimination from $[Mo^{VI}_2O_6(OBu)]^-$ or by subsequent isomerization seemed a more plausible interpretation. The ion previously assigned as $[Mo^{V}_2O_5(OH)]^-$ (*m*/*z* 289) is relabeled $[Mo_2, O_6, H]^-$ to emphasize its stoichiometry and the uncertainty of its structure.[50]

Previous theoretical studies suggest possible mechanisms for the formation of $[Mo_2, O_6, H]^-$ isomers. Allison and Goddard used generalized valence bond theory to study the interaction of methanol with a range of oxomolybdenum(VI) species.[14a] They concluded that the most likely mechanism for elimination of formaldehyde from binuclear oxomolybdenum (VI) species containing a methoxo ligand was transfer of hydrogen from the methoxo ligand to an oxo ligand of the *neighboring* metal center. However, they also suggested that direct abstraction of hydride by the molybdenum(VI) center was only slightly less favored at 300 °C, and could not be excluded as a possibility. Weber examined theoretically the elimination of formaldehyde from idealized fragments of metal-oxo clusters using extended Hückel theory.[14b] It was concluded that hydride transfer to the metal center was the first step in the elimination of formaldeyde and was followed by transfer of this hydrogen to an oxo ligand to form an hydroxo ligand.

These studies suggested possible mechanisms for elimination of aldehyde from $[Mo_2O_6(OCHR_2)]^-$ and formation of different isomers of $[Mo_2, O_6, H]^-$: (i) transfer of hydrogen from the α-position to an oxo group and 2e$^-$ reduction of the dimolybdate center, (ii) transfer of hydride from the α-position directly onto a metal center, or (iii) transfer of hydride from the α-position directly onto a metal center followed by subsequent transfer of this hydrogen to an oxo unit and 2e$^-$ reduction of the dimolybdate center. Although the isotope labeling experiments of eqs 2 and 15 did not distinguish between these mechanistic pathways, the kinetic data (Figure 8) suggested the formation

(47) The threshold voltage for this reaction is approximately 0.54 V_{p-p}. This can be compared with that required for dissociation of $[Mo_2O_6(OCH_3)]^-$ (Figure 6).

(48) The 20% of $[Mo_2, O_6, H]^-$ sample that is unreactive towards methanol and nitromethane represents a 'sink' in the catalytic cycles of Figure 1.

(49) The pressure of helium within the ion trap ($P_{He} \approx 1.75 \times 10^{-3}$ Torr) is about 4 orders of magnitude higher than the pressures of neutral reactants used in these experiments (typically, $P_{Neut} \approx 1.5 \times 10^{-7}$ Torr). Thus each ion undergoes an average of approximately 10^4 collisions with helium before collision with reactive neutrals. This would appear to be sufficient to cool the ions and provide a thermalised population of $[Mo_2, O_6, H]^-$ ions. To test this proposition, the rate of reaction was measured over a 10-fold range of methanol pressure, effectively varying the average number of collisions with helium before collision with methanol. Reaction rate was found to be independent of methanol pressure.

(50) In these experiments, $[Mo_2, O_6, H]^-$ is generated via CID of $[Mo_2O_6(O^nBu)]^-$ (eq 11, 18). Alternatively, $[Mo_2, O_6, H]^-$ can be generated via reactions 1 and 2 of cycle 1 (Figure 1). An unreactive component of $[Mo_2, O_6, H]^-$ is also observed using this method of synthesis, accounting for between 10 and 20% of the total ion current. The proportion of this unreactive component is expected to be sensitive to the nature of the alkoxo ligand of $[Mo_2O_6(OCHR_2)]^-$ and the degree of collisional activation used, but no attempts have been made to quantify the influence of these factors.

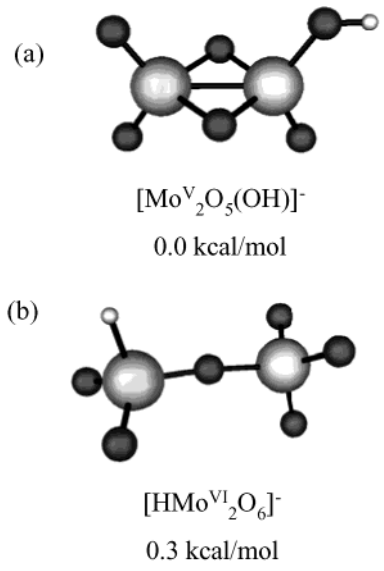

Figure 9. Predicted structural isomers for the ion of stoichiometry $[Mo_2, O_6, H]^-$(a) a di-μ-oxo-Mo^{V}_{2} species with a terminal hydroxo ligand; and (b) a μ-oxo-Mo^{VI}_{2} species with a terminal hydride ligand.

of two distinct $[Mo_2, O_6, H]^-$ isomers. Density functional theory (DFT) calculations have been used to investigate the relative stabilities of possible isomers of $[Mo_2, O_6, H]^-$ generated via these mechanisms.[51]

The most stable isomer of $[Mo_2, O_6, H]^-$ is predicted to be a di-μ-oxo-Mo^{V}_{2} species with a terminal hydroxo ligand and a formal Mo−Mo bond, $[Mo_2{}^{V}O_5(OH)]^-$ (Figure 9a). However, a μ-oxo-Mo^{VI}_{2} species featuring a terminal hydrido ligand $[HMo^{VI}_{2}O_6]^-$ is predicted to be only 0.3 kcal/mol higher in energy (Figure 9b). Mixed valence $Mo^{VI}Mo^{IV}$ species are all predicted to be at least a further 12 kcal/mol higher in energy (Fig. S12).[52] The most stable isomer, $[Mo^{V}_{2}O_5(OH)]^-$ (Figure 9a), possesses the Mo−OH unit implicated in reaction with methanol and is reduced, suggesting reduction of nitromethane is possible. Thus, in line with its previous assignment, $[Mo^{V}_{2}O_5(OH)]^-$ is proposed to be the reactive component of $[Mo_2, O_6, H]^-$, formed via abstraction of an α-hydrogen of the alkoxo ligand by an adjacent oxo ligand. The second most stable isomer, $[HMo^{VI}_{2}O_6]^-$ (Figure 9b), does not contain a Mo−OH unit and the metal atoms are in their highest oxidation state, suggesting reduction of nitromethane is less likely. This isomer is proposed as the unreactive component of $[Mo_2, O_6, H]^-$, formed via hydride abstraction by the metal center of an α-hydrogen of the alkoxo ligand.[53,54] These conclusions are discussed in more detail in the next section in the context of comparisons with the analogous chromium and tungsten centers.

Table 2. Reaction Rates for Reaction of $[M^{VI}_{2}O_6(OH)]^-$ (M = Cr, Mo, W) with CH_3OH

ion	k_{exp}[a]	reaction efficiency, ϕ[b]
$[Cr_2O_6(OH)]^-$	< 0.005	< 0.00003
$[Mo_2O_6(OH)]^-$	6.9	0.049
$[W_2O_6(OH)]^-$	78	0.57

[a] $\times 10^{-11}$ cm^3 molecules^{-1} s^{-1}. [b] $\phi = k_{exp}/k_{ado}$.

Comparison of the Reactivity of Dimolybdate Ions with Dichromate and Ditungstate Analogs. Dichromate can be generated and trapped in the gas phase via ESI of CH_3CN solutions of $(Bu_4N)_2[Cr_2O_7]$. However, the ditungstate dianion has not been isolated in the condensed phase.[55] It can be generated and trapped in the gas phase via ESI of CH_3CN solutions of $(Bu_4N)_2[WO_4]$ and is presumably formed via condensation of two monotungstate centers (eq 21).[56] Sufficient quantities of protonated ditungstate $[W_2O_6(OH)]^-$ and the ion-pair $\{Bu_4N^+[W_2O_7]^{2-}\}^-$ could be generated for subsequent gas-phase experiments. Consequently, comparison of reactivities of the chromium, molybdenum and tungsten congeners was possible for reactions relevant to the catalytic cycles of Figure 1

$$2\,[WO_4]^{2-} + 2\,H^+ \rightarrow [W_2O_7]^{2-} + H_2O \qquad (21)$$

Reaction 1. This first step in cycle 1 involves reaction of $[Mo_2O_6(OH)]^-$ with methanol (Figure 1). The rate of this reaction was compared with those for $[Cr_2O_6(OH)]^-$ and $[W_2O_6(OH)]^-$ (Table 2).

$[Cr_2O_6(OH)]^-$ did not react with methanol on the time scale and methanol concentrations used in these experiments, allowing an upper bound to be placed on its rate constant, i.e., $[Cr_2O_6(OH)]^-$ reacted with methanol *less than* once in every 30 000 collisions (ϕ < 0.000 03). In comparison, $[Mo_2O_6(OH)]^-$ reacted about once in every 20 collisions (ϕ = 0.049), representing a minimal 3 orders of magnitude increase in rate. $[W_2O_6(OH)]^-$ is a further order of magnitude more reactive than $[Mo_2O_6(OH)]^-$. Consequently, the first step of cycle 1 is not observed for $[Cr_2O_6(OH)]^-$ and proceeds most rapidly for $[W_2O_6(OH)]^-$ (Table 2).

The isotope labeling experiments for $[Mo_2O_6(OH)]^-$ with methanol (eq 1a−d) and reactions with alcohols of varying acidity (Table 1) were consistent with a mechanism involving deprotonation of the alcohol and elimination of hydroxo ligand as neutral water. This suggested that changes in basicity of the M−OH units in $[M_2O_6(OH)]^-$ (M = Cr, Mo, W) would affect reaction rate. The rate of reaction 1 increased down the group: Cr ≪ Mo < W (Table 2). This correlates with a decrease in the Sanderson electronegativity Cr^{VI} (3.37) > Mo^{VI} (2.20) > W^{VI} (1.67) and a consequent increase in M-OH basicity.[57]

Reaction 2. This reaction is common to cycles 1 and 2 (Figure 1) and involves elimination of aldehyde from $[Mo_2O_6(OCHR_2)]^-$. Collisional activation of $\{Bu_4N^+[M_2O_7]^{2-}\}^-$ ion-

(51) DFT has been used previously to study the related $[M_2O_7]^{2-}$ anions (M = Cr, Mo, W): (a) Amado, A. M.; Ribeiro-Claro, P. J. A. *J. Mol. Struct. (THEOCHEM)*, **1999**, *469*, 191 (b) Bridgeman, A. J.; Cavigliasso, G. *J. Phys. Chem. A* **2001**, *105*, 7111.

(52) These calculations address only the thermodynamic stability of possible isomeric forms of $[Mo_2, O_6, H]^-$. Given that these species are generated via collisional activation, kinetic considerations are also likely to be important in determining the relative populations of these isomers.

(53) The component of $[Mo_2, O_6, H]^-$ assigned as $[HMo^{VI}_{2}O_6]^-$ is also unreactive towards CH_3CO_2H (k_{exp} < 5 × 10^{-14} cm^3 molecule^{-1} s^{-1}). This isomer might be expected to react with acids via loss of H_2. For example, $[HCr(CO)_3]^-$ reacts with alcohols ROH to form $[ROCr(CO)_3]^-$ with loss of H_2 (Lane, K. R.; Squires, R. R. *J. Am. Chem. Soc.* **1985**, *107*, 6403). However, other metal hydrides are less reactive: $[(CH_3)_3AlH]^-$ only undergoes adduct formation with CF_3CH_2OH (Damrauer, R.; Krempp, M.; Damrauer, N. H.; Schmidt, M. W.; Gordon, M. S. *J. Am. Chem. Soc.* **1993**, *115*, 5218).

(54) Given the possibility of competing mechanisms of aldehyde elimination from $[Mo_2O_6(OCHR_2)]^-$, the kinetic isotope effect for elimination of CH_3CHO from $[Mo_2O_6(OCH_2CH_3)]^-$ described earlier may in fact be an *average* isotope effect for these two processes.

(55) (a) Errington, R. J.; Kerlogue, M. D. Richards, D. G. *Chem. Commun.* **1993**, 649 (b) Clegg, W.; Errington, R. J.; Fraser, K. A.; Richards, D. G. *Chem. Commun.* **1993**, 1105.

(56) Ditungstate species have been observed before using electrospray: see refs 6b,d.

(57) Huhey, J. E.; Keiter, E. A.; Keiter, R. L. *Inorganic Chemistry*, 4th ed.; Harper-Collins: New York, 1993; pp 188−190.

pairs (M = Cr, Mo, W; cf, eq 11) allowed generation of the respective $[M_2O_6(OBu)]^-$ anions and allowed exploration of their relative reactivities (eqs 22 and 23). Both $[Cr_2O_6(OBu)]^-$ and $[Mo_2O_6(OBu)]^-$ eliminated butanal upon collisional activation (eq 22) whereas $[W_2O_6(OBu)]^-$ underwent non-redox elimination of butene (eq 23, Fig S13). The clean elimination of alkene from $[Mo_2O_6(OC(CH_3)_3)]^-$ was observed previously in the absence of an α-hydrogen which prevented elimination of aldehyde (eq 19). In contrast, the presence of an α-hydrogen in $[W_2O_6(OBu)]^-$ suggested that alkene elimination is favored over aldehyde elimination for the tungsten congener. This contrasting behavior is consistent with the expected weaker oxidizing power of tungsten species compared to those of chromium and molybdenum[58]

$$[M^{VI}{}_2O_6(OBu)]^- \rightarrow [M_2, O_6, H]^- + CH_3CH_2CH_2CHO \quad (M = Cr, Mo) \quad (22)$$

$$[W^{VI}{}_2O_6(OBu)]^- \rightarrow [W^{VI}{}_2O_6(OH)]^- + CH_3CH_2CH{=}CH_2 \quad (23)$$

$[W_2O_6(OCH_3)]^-$ (generated via reaction of $[W_2O_6(OH)]^-$ with CH_3OH) does not contain a β-hydrogen. Consequently, alkene elimination is not possible and formaldehyde elimination was observed instead (eq 24). This reaction is analogous to reaction 2 of cycles 1 and 2 for the dimolybdate center (Figure 1). This confirms that elimination of aldehyde is possible for the ditungstate congener, but that the lower oxidizing power favors elimination of alkene where possible

$$[W^{VI}{}_2O_6(OCH_3)]^- \rightarrow [W_2, O_6, H]^- + H_2CO \quad (24)$$

The threshold voltage for elimination of formaldehyde from $[M_2O_6(OCH_3)]^-$ (M = Cr, W) can be compared with that described earlier for $[Mo_2O_6(OCH_3)]^-$ i.e., M = Cr (V_{p-p} = 0.38 V) < M = Mo (V_{p-p} = 0.61 V) < M = W (V_{p-p} = 0.77 V) (Figure 6).[59] These experiments suggest the general trend Cr < Mo < W, consistent with that based on the expected oxidizing power of the respective metal centers.[58]

Reactions 3 and 4. The final step of cycle 1 is the oxidation of $[Mo^V{}_2O_5(OH)]^-$ with nitromethane (Figure 1). $[Mo^V{}_2O_5(OH)]^-$ was also observed to react with methanol to form $[Mo^V{}_2O_5(OCH_3)]^-$ as part of cycle 2. In addition, samples of this ion contained an unreactive component (Figure 8). On the basis of DFT calculations, the reactive and unreactive components were assigned tentatively to $[Mo^V{}_2O_5(OH)]^-$ and $[HMo^{VI}{}_2O_6]^-$, respectively (Figure 9). Equivalent DFT calculations were carried out for the chromium and tungsten congeners (Table 3).

Reaction of $[Cr_2, O_6, H]^-$ (formed via eq 22) with methanol proceeded extremely slowly (ϕ = 0.000 30). In contrast to the molybdenum system, the reaction proceeded under smooth *pseudo* first-order kinetics with no evidence of an unreactive component. DFT calculations predicted the most stable isomer of $[Cr_2, O_6, H]^-$ to be the di-μ-oxo $Cr^V{}_2$ species with a terminal hydroxo ligand, $[Cr^V{}_2O_5(OH)]^-$ (Table 3). Mixed valence $Cr^{IV}Cr^{VI}$ centers were predicted to be at least 16 kcal/mol higher in energy, while the μ-oxo $Cr^{VI}{}_2$ center with a terminal hydrido ligand $[HCr^{VI}{}_2O_6]^-$ was predicted to be 41 kcal/mol higher in energy (Figure S14). The most stable isomer, $[Cr^V{}_2O_5(OH)]^-$, has the equivalent structure to that assigned as the reactive component of $[Mo_2, O_6, H]^-$. This prediction is consistent with the experimental observation that the chromium system reacts completely with methanol, with no evidence of an unreactive component. The ion of stoichiometry $[Cr_2, O_6, H]^-$ is assigned tentatively to $[Cr^V{}_2O_5(OH)]^-$.

The reactivity of $[Cr^V{}_2O_5(OH)]^-$ can be compared with that of $[Cr^{VI}{}_2O_6(OH)]^-$ and $[Mo^V{}_2O_5(OH)]^-$. Reaction of $[Cr^V{}_2O_5(OH)]^-$ with methanol (ϕ = 0.000 30) is *at least* an order of magnitude faster than that of $[Cr^{VI}{}_2O_6(OH)]^-$ (ϕ < 0.000 03). This correlates with the expected increased basicity of hydroxo ligand and the lower steric barriers for $[Cr^V{}_2O_5(OH)]^-$. The reactive component of $[Mo_2, O_6, H]^-$, assigned as $[Mo_2O_5(OH)]^-$, is approximately 3000 times more reactive toward methanol than $[Cr_2O_5(OH)]^-$. This is presumably for similar reasons to those which cause the oxidized $[Mo^{VI}{}_2O_6(OH)]^-$ center to be at least 3 orders of magnitude more reactive than $[Cr^{VI}{}_2O_6(OH)]^-$ (Table 2).

While $[W_2, O_6, H]^-$ cannot be generated via collisional activation of $[W_2O_6(OBu)]^-$ (eq 23), it can be generated via collisional activation of $[W_2O_6(OCH_3)]^-$ (eq 24). $[W_2, O_6, H]^-$ was unreactive toward methanol on the time scale and concentrations used in these experiments, allowing an upper bound to be placed upon the rate constant (k_{exp} < 5.0 × 10^{-14} cm^3 $molecule^{-1}$ s^{-1}). This contrasted with the rapid reaction of $[W_2O_6(OH)]^-$ with methanol (ϕ = 0.57, Table 2). Further, the reactive component of $[Mo_2, O_6, H]^-$, assigned to $[Mo^V{}_2O_5(OH)]^-$, reacted at the collision rate with methanol. DFT calculations predicted the most stable isomer of $[W_2, O_6, H]^-$ to be the μ-oxo-$W^{VI}{}_2$ center with a terminal hydride ligand, $[HW^{VI}{}_2O_6]^-$ (Table 3). Mixed valence species are predicted to be at least 19 kcal/mol higher in energy, and $[W^V{}_2O_5(OH)]^-$ is predicted to be approximately 21 kcal/mol higher in energy (Figure S15). This most stable hydride isomer has a structure equivalent to that assigned to the unreactive component of $[Mo_2, O_6, H]^-$ (Figure 9b). This prediction is consistent with the experimental observation that $[W_2, O_6, H]^-$ is unreactive toward methanol. This ion is now assigned as $[HW^{VI}{}_2O_6]^-$. Its stability correlates with the weaker oxidizing power of tungsten centers.

The reactivities of the chromium and tungsten systems (assigned as $[Cr^V{}_2O_5(OH)]^-$ and $[HW^{VI}{}_2O_6]^-$) toward nitromethane were also explored. Neither reduced nitromethane. An upper bound can be placed on their rate constant (k_{exp} < 5.0 × 10^{-14} cm^3 $molecule^{-1}$ s^{-1}). The inertness of $[Cr^V{}_2O_5(OH)]^-$ is consistent with it being a poorer reductant than $[Mo_2{}^VO_5(OH)]^-$, while that of $[HW^{VI}{}_2O_6]^-$ is consistent with its maximum oxidation state.

Table 3. Predicted Stability of $[HM^{VI}{}_2O_6]^-$ Isomer Relative to $[M^V{}_2O_5(OH)]^-$ Isomer (kcal/mol) for $[M_2, O_6, H]^-$ (M = Cr, Mo, W)

metal centre	$[M^V{}_2O_5(OH)]^-$ [a]	$[HM^{VI}{}_2O_6]^-$ [b]	reactive proportion
Cr	0.0	41.2	100
Mo	0.0	0.3	80
W	0.0	−21.3	0

[a] Corresponds to structure of Figure 9a. [b] Corresponds to structure of Figure 9b.

(58) (a) Brownstein, S.; Heath, G. A.; Sengupta, A.; Sharp, D. W. A. *Chem. Commun.* **1983**, 669 (b) Heath, G. A.; Moock, K. A.; Sharp, D. W. A.; Yellowlees, L. J. *Chem. Commun.* **1985**, 1503.

(59) $[Cr_2O_6(OCH_3)]^-$ cannot be generated via reaction of $[Cr_2O_6(OH)]^-$ with CH_3OH (Table 2). Instead, this ion was generated via reaction of $[Cr_2O_7]^{2-}$ with CH_3I.

Comparison of Reactivity of Mononuclear Species, $[MO_3(OH)]^-$ (M = Cr, Mo, W). To evaluate the importance of the binuclear nature of these group VI oxoanions in reactions relevant to catalytic cycles 1 and 2 of Figure 1, the reactivity of the analogous mononuclear systems, $[M^{VI}O_3(OH)]^-$ (M = Cr, Mo, W) was examined. These ions were generated by ESI of $(Bu_4N)_2[MO_4]$ (M = Cr, Mo, W) in CH_3CN.

Reaction 1. The first reaction of cycle 1 involves reaction of $[Mo_2O_6(OH)]^-$ with methanol. Each of the $[MO_3(OH)]^-$ ions was inert to reaction with methanol on the time scale and methanol concentrations used in these experiments. An upper bound could be placed on the rate constants for their reaction ($k_{exp} < 5 \times 10^{-14}$ cm^3 molecule^{-1} s^{-1}).[60] This represents *at least* a 3 orders of magnitude decrease over the binuclear dimolybdate and ditungstate systems (Table 3), reinforcing the importance of the second metal center in reaction 1 of cycle 1.

Reaction 2. Reaction 2 is the elimination of formaldehyde from $[Mo_2O_6(OCH_3)]^-$. Although the equivalent methoxo mononuclear centers cannot be generated via reaction of $[MO_3(OH)]^-$ with methanol, they can be generated and trapped in the gas phase via ESI of CH_3CN solutions of $(Bu_4N)_2[MO_4]$ (M = Cr, Mo, W) containing methanol (1% v/v). The reactivities of these species upon collisional activation were explored. $[CrO_3(OCH_3)]^-$ eliminated formaldehyde (eq 25), as observed for the analogous binuclear species, $[Cr_2O_6(OCH_3)]^-$, and is consistent with the known strong oxidizing power of mononuclear Cr(VI) centers. No reaction was observed for the mononuclear molybdenum and tungsten centers. Attempts to use higher collisional activation energies resulted in loss of ion signal. This may be due to electron detachment, formation of an ionic species whose mass is too low to be detected, or simply loss of ions from the ion trap. Although the lack of an observed reaction does not strictly rule out the possibility for aldehyde elimination, it demonstrates that a higher activation energy is required than that for aldehyde elimination from $[CrO_3(OCH_3)]^-$ and the relevant binuclear centers

$$[CrO_3(OCH_3)]^- \rightarrow [Cr, O_3, H]^- + H_2CO \qquad (25)$$

The elimination of alkenes is possible for alkoxo ligands other than methoxo. This was observed previously for the molybdenum binuclear centers with alkoxo ligands lacking an α-hydrogen (eq 19) or in the case of ditungstate where alkene elimination was favored over aldehyde elimination (eq 23). This possibility was examined for the mononuclear centers via the ethoxo ligands (eqs 26 and 27). The chromium center eliminated acetaldehyde (eq 26), consistent with elimination of formaldehyde from $[CrO_3(OCH_3)]^-$ (eq 25). The mononuclear molybdenum center eliminated ethene in a nonredox reaction (eq 27), contrasting with the elimination of acetaldehyde by binuclear $[Mo_2O_6(OCH_2CH_3)]^-$ (eq 15). These differing reactivities reinforce the importance of the second metal center in reaction 2 of cycles 1 and 2. The mononuclear tungsten center also eliminated the ethoxide ligand as ethene (eq 27), as observed for the binuclear ditungstate center (e.g., eq 23)

$$[Cr^{VI}O_3(OCH_2CH_3)]^- \rightarrow [Cr, O_3, H]^- + CH_3CHO \qquad (26)$$

$$[M^{VI}O_3(OCH_2CH_3)]^- \rightarrow [M^{VI}O_3(OH)]^- + CH_2{=}CH_2 \quad (M = Mo, W) \qquad (27)$$

Neither of the first two steps of cycle 1 (Figure 1) proceeded with the mononuclear molybdate center. The difference in reactivity between mononuclear molybdate and binuclear dimolybdate reinforces the importance of the second MoO_3 unit in the sequence of reactions observed in the catalytic cycles of Figure 1.

Conclusions

Two gas-phase catalytic cycles are presented for the oxidation of primary and secondary alcohols to aldehydes and ketones, respectively, with a binuclear dimolybdate center acting as the catalyst (Figure 1). Cycle 1 proceeds via three steps: **(1)** activation of the alcohol to form an alkoxo-molybdenum bond with elimination of water; **(2)** oxidation of the alkoxo ligand and its elimination as aldehyde upon collisional activation in the rate-determining step; and **(3)** regeneration of the catalyst via oxidation by nitromethane. Cycle 2 shares reaction 2 in common with cycle 1, but differs in the sequence of reaction with alcohol and nitromethane.

The nature of these reactions was probed by kinetic measurements, by variation of the substrate alcohols (structure and isotope labeling) and by variation of the reactive center (metal and nuclearity). The molybdenum and tungsten binuclear centers $[M_2O_6(OH)]^-$ (M = Mo, W) promoted reaction 1 but the chromium center $[Cr_2O_6(OH)]^-$ did not (Table 2). This is consistent with the expected order of basicity of the hydroxo ligand in these species. In general, the chromium and molybdenum centers $[M_2O_6(OCHR_2)]^-$ (M = Cr, Mo) promoted reaction 2, but the tungsten centers $[W_2O_6(OCHR_2)]^-$ did not. This is consistent with the expected order of oxidizing power of the anions.

Evidence was presented that the product of reaction 2 involves structural isomers of stoichiometry $[Mo_2, O_6, H]^-$. Approximately 80% of the sample of $[Mo_2, O_6, H]^-$ reacted with nitromethane in reaction 3 (cycle 1) and with methanol in reaction 4 (cycle 2), whereas the remaining 20% was unreactive to both neutrals. DFT calculations suggest that at least two structural isomers may be accessible (Figure 9). The reactive form of $[Mo_2, O_6, H]^-$ is assigned to $[Mo^V_2O_5(OH)]^-$ and the unreactive form to $[HMo^{VI}_2O_6]^-$. The experimental observations are consistent with the expected relative reactivities of these isomers. Calculations also predicted that the reduced $[Cr^V_2O_5(OH)]^-$ isomer is favored for chromium, whereas the hydride form $[HW^{VI}_2O_6]^-$ is favored for tungsten. These assignments are consistent with the greater oxidizing power expected for chromium(VI) relative to tungsten(VI), and are consistent with the observed reactivities of $[Cr^V_2O_5(OH)]^-$ and $[HW^{VI}_2O_6]^-$ toward methanol and nitromethane.

The experiments revealed that only the dimolybdate center has the mix of properties that allow it to participate in *each* of the three steps required by cycles 1 and 2. Although the dichromate congener is the strongest oxidant, it is the weakest base, making it unreactive toward alcohols. By contrast, the ditungstate congener is the strongest base, but its weaker

(60) Given the order of magnitude rate increase of CF_3CH_2OH over methanol towards $[Mo_2O_6(OH)]^-$ (Table 1), we have also investigated the reactivity of these mononuclear centres towards CF_3CH_2OH. $[CrO_3(OH)]^-$ is unreactive towards CF_3CH_2OH under our experimental conditions, while $[MoO_3(OH)]^-$ and $[WO_3(OH)]^-$ each undergo extremely slow reaction to form $[MO_3(OCH_2CF_3)]^-$ (M = Mo, W). The rate of reaction was too slow to be measured with the present instrument ($k_{exp} < 5 \times 10^{-14}$ cm^3 molecule^{-1} s^{-1}). Clustering reactions to produce $[MO_3(OH){-}CF_3CH_2OH]^-$ were also observed (M = Mo, W).

oxidizing power means it prefers the non-redox elimination of alkene rather than aldehyde.

Each of the mononuclear anions $[MO_3(OH)]^-$ (M = Cr, Mo, W) was inert to reaction with methanol. $[CrO_3(OCH_2CH_3)]^-$ eliminated acetaldehyde, whereas the molybdenum and tungsten equivalents eliminated ethene in a non-redox reaction. This behavior contrasted with the elimination of acetaldehyde from binuclear $[Mo_2O_6(OCH_2CH_3)]^-$. The difference in reactivity between the mononuclear and binuclear molybdenum anions reinforces the importance of the second MoO_3 unit in the sequence of reactions of catalytic cycles 1 and 2.

The three reactions which constitute cycle 1 are equivalent to the three essential steps proposed to occur in the industrial oxidation of gaseous methanol to formaldehyde over molybdenum(VI)-trioxide solid-state catalysts at 300−400 °C (see Introduction above). A number of comparisons can be made between the catalytic cycles of the present gas phase work and that of the industrial process:

(i) The rate-limiting step is elimination of aldehyde in each system. In the present gas phase study, reaction 2 does not proceed at room temperature, and the use of collisional activation is required. Similarly, no reactivity is observed at room temperature in the industrial process, and the use of elevated temperatures is required.

(ii) The oxidation of ethanol to acetaldehyde over a variety of supported molybdenum(VI)-trioxide catalysts at temperatures between 410 °C and 510 °C has been investigated.[61] From a comparison of turnover rates for CH_3CD_2OH and CH_3CH_2OH, an isotope effect in the range of 1.7−2.2 was estimated. The kinetic isotope effect of 1.9 ± 0.4 for the elimination of acetaldehyde from $[Mo_2O_6(OCHDCH_3)]^-$ in the present study matches that estimate.

(iii) Temperature programmed desorption has been used to study the effect of alcohol structure on the products of reaction over molybdate solid-state catalysts.[15] The only products detected for *t*-BuOH were 2-methyl-propene and water from the nonredox dehydration reaction. The elimination of 2-methyl-propene from $[Mo_2O_6(OC(CH_3)]^-$ observed in the present work (eq 19) is consistent with these observations. Further, temperature programmed desorption experiments suggest branched alcohols such as *i*-propanol result in increased yield of the alkene versus the aldehyde, also consistent with observations from the present study (eq 17).

(iv) The catalytic activities of ferric tungstate $Fe_2(WO_4)_3$ and ferric molybdate $Fe_2(MoO_4)_3$ have been compared for the oxidation of methanol.[62] Although the reaction rates were similar, the tungsten system produced mainly dimethyl ether via a nonredox process, whereas the molybdenum system evolved mainly formaldehyde via the redox process. These observations are consistent with those from the present work where the weaker oxidizing power of tungsten led to a preference for alkene elimination compared to aldehyde elimination in the molydenum analogue (eq 22, 23). Polyoxotungstate systems have also been shown to be effective catalysts for the dehydration of ethanol to ethylene in a *pseudo*-liquid phase.[63]

(v) Oxo−Mo^{VI} binuclear units on SiO_2 supports were prepared by reaction of $Mo_2(\eta^3\text{-}C_3H_5)_4$ with SiO_2, followed by successive reaction with H_2 and O_2.[64] This method allowed assembly of well-defined adjacent MoO_4 units on the SiO_2 surface. This catalyst showed an order of magnitude higher activity than molybdate catalysts prepared via conventional impregnation methods. The observation was rationalized in terms of a "cooperative effect" between the two units of a binuclear molybdate center. An ethanol molecule was proposed to condense onto a single molybdate unit to form an ethoxo-Mo(VI) center, followed by elimination of acetaldehyde via abstraction of an α-hydrogen of the ethoxo ligand by the *neighboring* molybdate center. Results from the present study indicating that mononuclear molybdate centers are ineffective but that binuclear centers are effective for the elimination of aldehyde are consistent with this proposal.

(vi) The compound $Mo^{VI}_2O_5(OCH_3)_2$ has been proposed as a model heterogeneous catalyst.[11c] Its layered structure features *trans*-$Mo^{VI}O(OCH_3)$ units which are perpendicular to the layer planes and are separated by in-plane bridging oxo ligands. Neighboring units alternate in their orientation relative to the plane. A mechanism of formaldehyde elimination similar to that proposed for the binuclear centers in the present work is easily envisaged, involving adjacent Mo^{VI} centers within one layer plane or between adjacent planes. Oxygen vacancies created by formaldehyde elimination from adjacent Mo^{VI} centers would be amenable to regeneration by the two O atoms available from O_2. The presence of adjacent oxygen-deficient units in the solid-state catalyst should expedite reaction with O_2.

(vii) The observation of a second catalytic cycle in the present work differing in the sequence of reaction with methanol and nitromethane suggests related reactions may also occur in reverse order in the industrial process. This proposal could be tested using temperature programmed desorption experiments.[15]

Acknowledgment. T.W. acknowledges the support of an Australian Postgraduate Award and a Melbourne Abroad Travel Scholarship, and thanks Professor Mark Gordon and Dr. Mike Schmidt for hosting a visit and assistance with the use of GAMESS. T.W. and R.A.J.O. thank Professor Scott Gronert for helpful discussions concerning rate measurements. R.A.J.O. thanks the Australian Research Council for financial support (Grant No. A00103008) and the University of Melbourne for funds to purchase the LCQ. R.A.J.O. also thanks Professors Peter Armentrout and Michael Bruce for interesting discussions and helpful suggestions. Reviewers are thanked for their helpful comments and suggestions.

Supporting Information Available: Relevant mass spectra (see text), Cartesian coordinates and energies of $[M_2, O_6, H]^-$ isomers (M = Cr, Mo, W). This material is available free of charge via the Internet at http://pubs.acs.org.

JA028839X

(61) Zhang, W.; Oyama, S. T. *J. Phys. Chem.* **1996**, *100*, 10 759.
(62) Harrison, W. T. A.; Chowdhry, U.; Machiels, C. J.; Sleight, A. W.; Cheetham, A. K. *J. Solid State. Chem.* **1985**, *60*, 101.
(63) Lee, K. Y.; Arai, T.; Nakata, S.; Asaoka, S.; Okuhara, T.; Misono, M. *J. Am. Chem. Soc.* **1992**, *114*, 2836.
(64) Iwasawa, Y. In *Tailored Metal Catalysts*; Iwasawa, Y. Eds.; D. Reidel Publishing Company: Holland, **1986**, p 54−60 and references therein.